

EFFECT OF RADIATION DAMAGE ON THE
FORMATION OF MULLITE IN KAOLINITE

A THESIS

Presented to
the Faculty of the Graduate Division
by

Clarence McMahan Head

In Partial Fulfillment of the
Requirements for the Degree
Master of Science in Ceramic Engineering

Georgia Institute of Technology

November, 1964

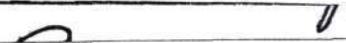

In presenting the dissertation as a partial fulfillment of the requirements for an advanced degree from the Georgia Institute of Technology, I agree that the Library of the Institute shall make it available for inspection and circulation in accordance with its regulations governing materials of this type. I agree that permission to copy from, or to publish from, this dissertation may be granted by the professor under whose direction it was written, or, in his absence, by the Dean of the Graduate Division when such copying or publication is solely for scholarly purposes and does not involve potential financial gain. It is understood that any copying from, or publication of, this dissertation which involves potential financial gain will not be allowed without written permission.

3/17/65

b

EFFECT OF RADIATION DAMAGE ON THE
FORMATION OF MULLITE IN KAOLINITE

Approved:

Date Approved by Chairman:

June 1, 1965

ACKNOWLEDGMENTS

The author wishes to thank the Edward Orton Jr. Ceramic Foundation and the Georgia Institute of Technology for funds which made the investigation possible, the Atomic Energy Commission for use of the Ce^{137} irradiator, and the Lockheed-Georgia Company for use of its computer.

The author would like to express his appreciation to Doctor R. A. Young and his staff for their interest and technical assistance. He is also indebted to Doctors W. E. Moody and Lane Mitchell for their advice and cooperation, and to Messrs. W. J. Corbett and J. H. Burson for their helpful discussions and samples provided.

TABLE OF CONTENTS

	Page
ACKNOWLEDGMENTS	ii
LIST OF TABLES	iv
LIST OF FIGURES	v
ABSTRACT	vi
Chapter	
I. INTRODUCTION	1
II. REVIEW OF LITERATURE	2
III. PROCEDURE	12
IV. DISCUSSION OF RESULTS	35
V. CONCLUSIONS	42
APPENDICES	
A. GRAIN SIZE DISTRIBUTION OF KAOLINITE SAMPLES	43
B. CALCULATION OF ERRORS	45
C. MULLITE GROWTH DATA	47
D. ATTEMPTS TO DETERMINE THE MULLITE ACTIVATION ENERGY	60
BIBLIOGRAPHY	65

LIST OF TABLES

Table		Page
1.	X-Ray Fluorescence Analysis for Metal Impurities in Kaolinite (After Electrodialysis).	15
2.	Irradiation Doses	17
3.	Crystallinity Index Determinations.	19
4.	Mullite Growth--1200°C.	48
5.	Mullite Growth--1150°C.	52
6.	Mullite Growth--1100°C.	56

LIST OF FIGURES

Figure		Page
1.	Crystal Structure of Kaolinite.	4
2.	Effect of nb/3 Shifting	4
3.	X-Ray Diffraction Pattern of Well nb/3-Crystallized Kaolinite.	6
4.	X-Ray Diffraction Pattern of Poorly nb/3-Crystallized Kaolinite.	7
5.	Crystal Structure of Mullite.	10
6.	Electrodialysis Cell Schematic.	14
7.	nb/3-Crystallinity Changes by Irradiation	20
8.	Schematic of High Temperature Diffraction Unit.	22
9.	Diffraction Patterns of Sillimanite-Mullite Growth from Poorly nb/3-Crystallized Kaolin (10^{22} ev)	26
10.	A. Sillimanite-Mullite Growth from Well nb/3-Crystallized Kaolin	27
	B. Sillimanite-Mullite Growth from Medium nb/3-Crystallized Kaolin	28
	C. Sillimanite-Mullite Growth from Poorly nb/3-Crystallized Kaolin	29
11.	Electron Microscope Studies of Mullite Growth from Poorly nb/3-Crystallized Kaolin.	32
12.	Electron Microscope Studies of Mullite Growth from Medium nb/3-Crystallized Kaolin.	33
13.	Electron Microscope Studies of Mullite Growth from Well nb/3-Crystallized Kaolin.	34
14.	Particle Size Distribution of Sample Clays.	44

ABSTRACT

The effects of gamma irradiation on the clay mineral kaolinite were observed through (1) changes in the kaolinite nb/3-crystallinity*, as ascertained by measures of nb/3 shifting, and (2) the kinetics of the kaolinite-mullite transformation, in relation both to reaction rate and to quantity of mullite formed.

Three kaolinites with varying degrees of nb/3-crystallinity were irradiated by 0.67 mev gamma-rays from a Ce^{137} source. The effect of the various dosages on the crystallinity of each kaolinite was determined to be as follows: (1) for doses up to 10^{19}ev/gm (ferrous ion solution) a slight improvement of the nb/3-crystallinity was observed, and (2) the nb/3-crystallinity decreased progressively with increasing dosage greater than $\approx 10^{19}\text{ev/gm}$. The probable mechanism producing this radiation damage (nb/3-crystallinity change) was random nb/3 Al ion movement (induced by Compton electrons).

The use of gamma radiation provided an attractive method of determining virtually only the effect of nb/3-crystallinity on the formation of mullite, as the effects of most other variables (such as impurity content) were essentially held constant. By means of high temperature X-ray diffractometry it was ascertained that, on firing, the clays irradiated with doses up to 10^{19}ev/gm developed a mullite content approximately 5

* This rather cumbersome term is advanced to avoid the ambiguities which arise from the common practice of using the less specific expression, crystallinity, for the same purpose.

per cent greater than that developed in the unirradiated clay. This mild irradiation also increased the mullite formation rate. For those samples in which the nb/3-crystallinity was lowered by doses in excess of 10^{19} ev/gm, X-ray diffractometry indicated a range of 1 to 15 per cent decrease in final mullite content, and a decreased formation rate (below that of the unirradiated clay).

The observed reversal in the dependence of mullite content and formation kinetics on radiation dosage is interpreted as being caused by the action of two competing processes: (1) gamma-ray induced increases in lattice energy through production of point defects, and (2) lowering of the nb/3-crystallinity by nb/3 shifting of Al ions (with little or no accompanying increase in lattice energy relative to mullite formation). The first effect tends to enhance mullite formation; the second retards it. The first effect is probably the predominant one for doses up to 10^{19} ev/gm; the nb/3-crystallinity effect becomes dominant for larger doses.

The dependence of the growth rate and of the quantity formed on the disordering of the Al ions (or decrease in $\frac{nb}{3}$ - crystallinity) due to high irradiation-doses appears to constitute evidence that preferentially oriented mullite growth from kaolinite is energetically favored to a measurable degree and is adversely affected by nb/3 shifting of the Al ions.

CHAPTER I

INTRODUCTION

Forming at temperatures in excess of 900°C, mullite is the crystalline end product of kaolinite thermal decomposition. Interlocking mullite crystals and mullite solid solutions are the prime contributors to clayware strength and heat resistance.

Mullite formation from kaolinite (kaolin) is dependent upon several factors. The primary factors include the type and concentration of impurities present, the crystallinity of the parent kaolin, and the kaolin grain size.

The purpose of this work was to determine the effects of exposure of kaolinite to gamma-rays on: (1) the kaolinite crystallinity as ascertained by measures of nb/3 shifting, and (2) the kinetics of mullite formation in relation both to growth rates and to quantity formed.

CHAPTER II

REVIEW OF LITERATURE

Kaolinite and Radiation Damage

Kaolinite Structure

Kaolinite is represented chemically as $\text{Al}_2\text{O}_3 \cdot 2\text{SiO}_2 \cdot 2\text{H}_2\text{O}$.

Brindley (1) states that kaolinite is triclinic with axial dimensions of $\underline{a} = 5.16 \text{ \AA}$, $\underline{b} = 8.97 \text{ \AA}$, $\underline{c} = 7.38 \text{ \AA}$, $\alpha = 91.8^\circ$, $\beta = 104.5^\circ$, $\gamma = 90^\circ$.

Structurally, kaolinite consists of two parallel layers alternately stacked one above the other, as shown in Fig. 1 (after Grim (2)). The first layer consists of silica tetrahedra arranged in a continuous series of ring structures; the second consists of alumina octahedra, in which hydroxyl ions occupy all of the anion sites in the unshared level and occur at intervals of $\underline{b}/3$. In the level of octahedral-tetrahedral conjunction only one-third of the anion sites are hydroxyl, the remainder are oxygen. For kaolinite to maintain electrical neutrality, only two-thirds of the crystal aluminum sites are occupied. Ideally the occupied Al sites have a continuous hexagonal structure in the \underline{a} and \underline{b} directions. In actuality some randomness in the distribution of Al ions among octahedral positions usually exists.

Kaolinite Crystallinity and Radiation Damage

The crystallinity of kaolinite is generally considered a measure of structural order. Disorders such as random layer displacements,

foreign ion substitutions, ionic displacements, interlayer water, etc., lower crystallinity. The term $nb/3$ -crystallinity is here applied to a specific type of order, destruction of which occurs by either of two crystallographically equivalent mechanisms: (1) shifts of entire kaolinite alumina layers by intervals of magnitude $nb/3$, as proposed by Brindley (3), and/or (2) shifts of individual aluminum ions along \vec{b} (or 120° on either side) into vacant lattice sites.

The effect of $nb/3$ layer shifting is shown in Fig. 2. In a perfectly crystallized kaolinite, the atoms of layer A lie above those of layer B (with the inclination of the \underline{c} - axis). In the shift shown $n = 1$), it is evident the atoms of layer B are no longer below those of layer A, but must move $2b/3$ units to the right or one $b/3$ units to the left before the layers are again aligned. The electrical balance of the crystal is not upset during the shift because displacements of $nb/3$ do not alter the near neighbor relation between layers. Kaolinite layer shifting, though common in nature, is an improbable effect of gamma-irradiation because of the energy requirements involved.

Displacements of individual aluminum ions may be due to any one of several mechanisms. These include ion displacements due to gamma-ray collision, Compton electrons, and the electron excitation (and energy dissipation) method proposed by Seitz (4). For 0.67 mev gamma-rays incident on aluminum, the Compton electron mechanism is more likely because the Compton process cross-section is more than 400 times that for the photoelectric process.

Indications of the degree of $nb/3$ -crystallinity can be obtained by use of the X-ray diffractometer. Murray (5) has related the degree

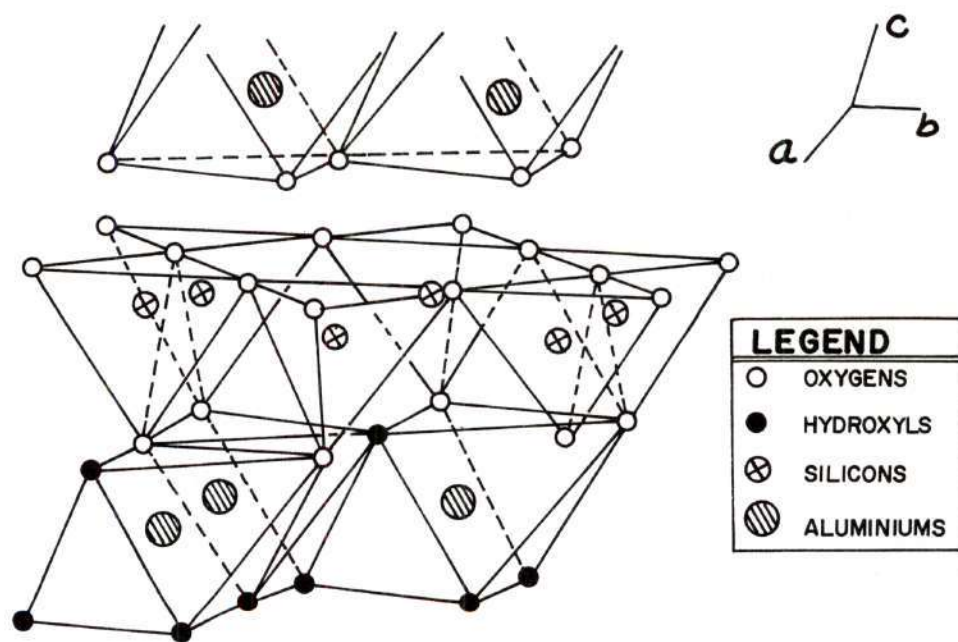


Figure 1. Crystal Structure of Kaolinite.

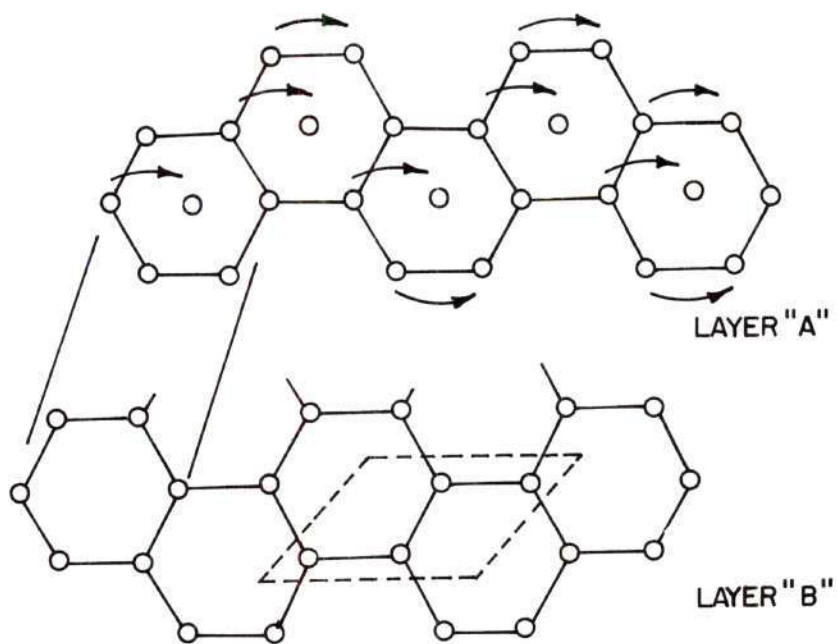


Figure 2. Effect of $nb/3$ Shifting.

of nb/3-crystallinity to the following points of a diffractometer trace: (1) slight increases in the basal spacing (particularly the (001) reflections), (2) resolution of the closely spaced reflections, (3) definition of the reflections, and (4) number of reflections. Kaolinites with high nb/3-crystallinity tend to have more reflections than do those of poorer nb/3-crystallinity. The poorly defined or diffuse reflections observed on the diffraction patterns of poorly nb/3-crystallized kaolinites may be related to Al ion movement. Diffraction patterns of well and poorly nb/3-crystallized kaolinites may be seen in Figs. 3 and 4. Brindley (6) has pointed out that when nb/3 displacements occur, the (hkl) reflections for which $k \neq 3n$ appear to be weakened or completely missing. A marked assymetry due to two-dimensional character in the diffraction pattern also develops in the reflections.

Johns and Murray (7) have devised an nb/3-crystallinity index for kaolinite based upon the ratio of the $(02\bar{1})/(060)$ reflection intensities of X-ray diffraction patterns. The $(02\bar{1})$ reflection is affected by nb/3 shifting of the Al ions; the (060) is not. The ratio varies from 0.0 for poorly nb/3-crystallized kaolinite to 1.0 (or slightly more) for a well nb/3-crystallized one.

The Formation of Mullite

Kaolinite-Mullite Reaction Series

Kaolinite crystals undergo structural changes upon dehydration. Observations by Brindley and Nakahira (8) indicate that the phase transformation begins in the vicinity of 470°C; the reaction proceeds as follows:

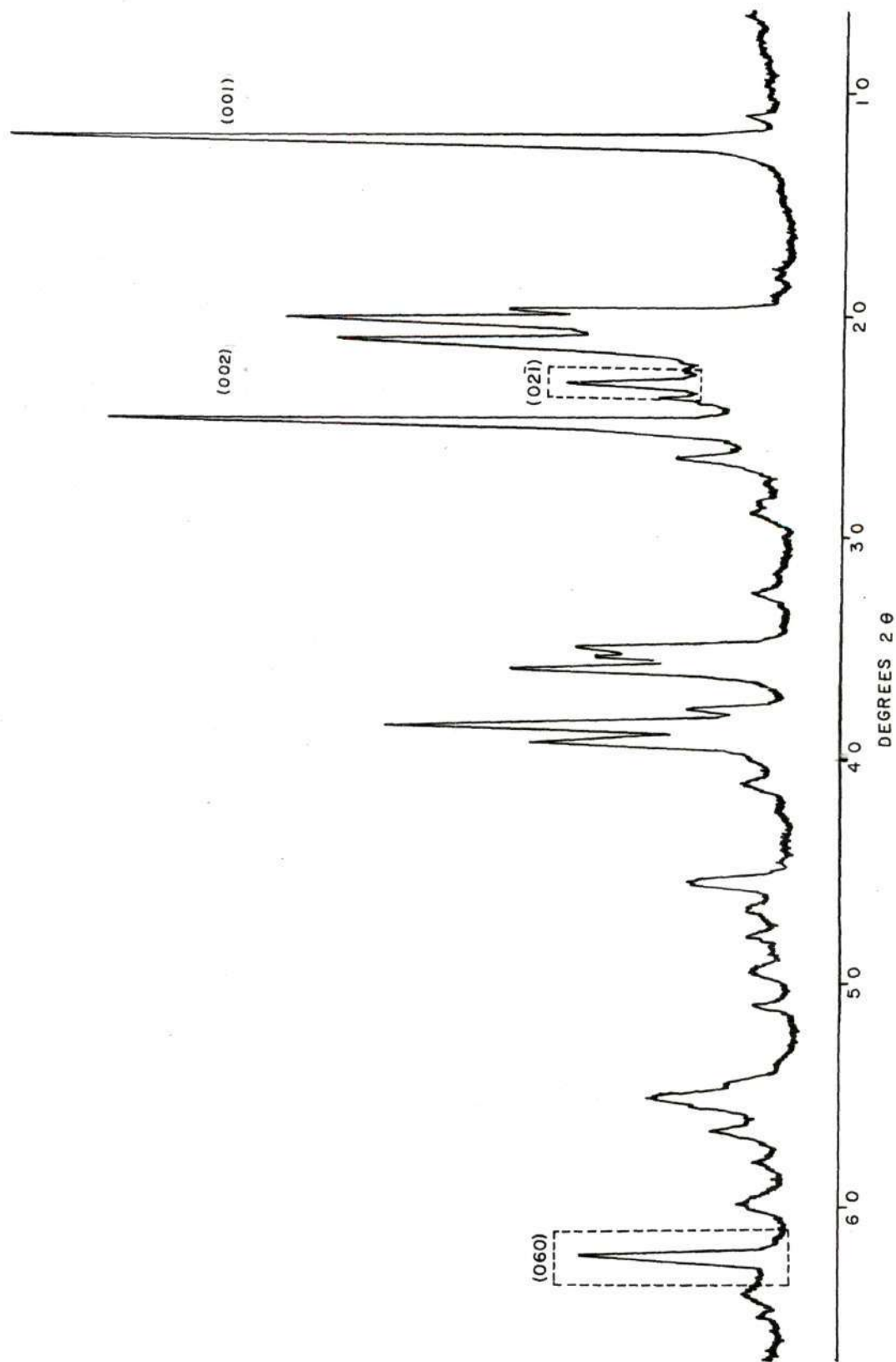


Figure 3. X-Ray Diffraction Pattern of Well nb/3-Crystallized Kaolinite.

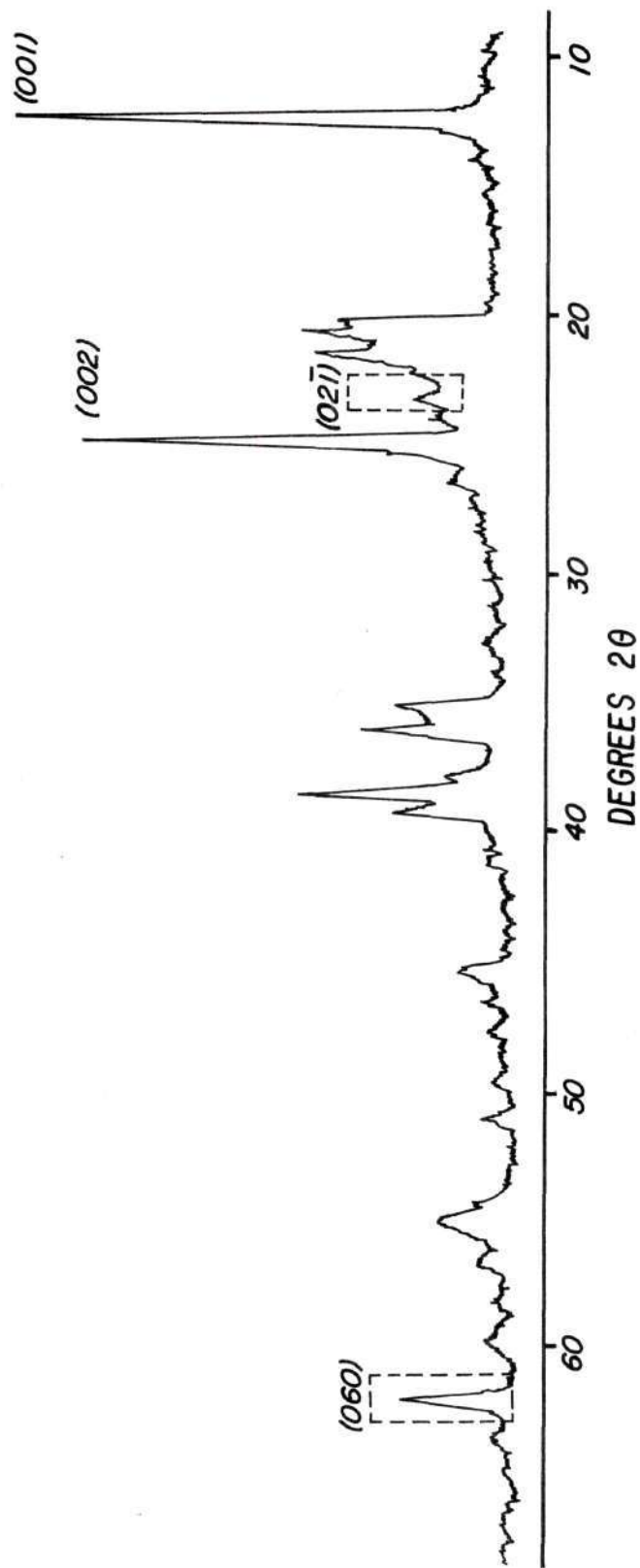
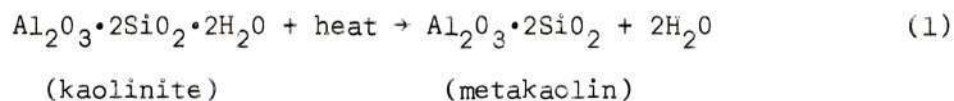
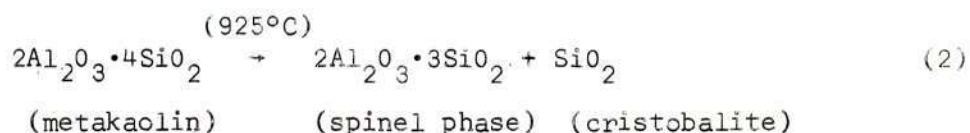


Figure 4. X-Ray Diffraction Pattern of Poorly nb/3-Crystallized Kaolinite.



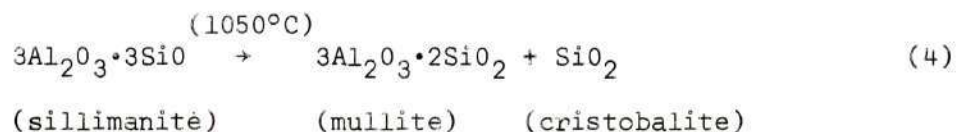
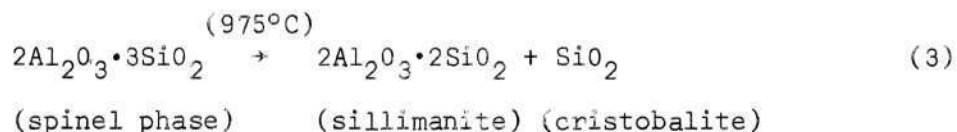
The regularity in the a and b directions of the kaolinite is carried forward to this transition phase. Periodicity in the c dimension disappears upon the removal of the (OH) ions. The coordination of the aluminum ions becomes tetrahedral.

Continued heating of the metakaolin phase produces a second phase transformation:



The important feature of the spinel phase (cubic) is the restoration of the c - axis periodicity (particularly with respect to the Al ions). The aluminum ions are octahedrally coordinated and form continuous chains parallel to the kaolinite \vec{b} . The presence of cristobalite does not usually become evident on the X-ray diffractometer patterns below 1000°C.

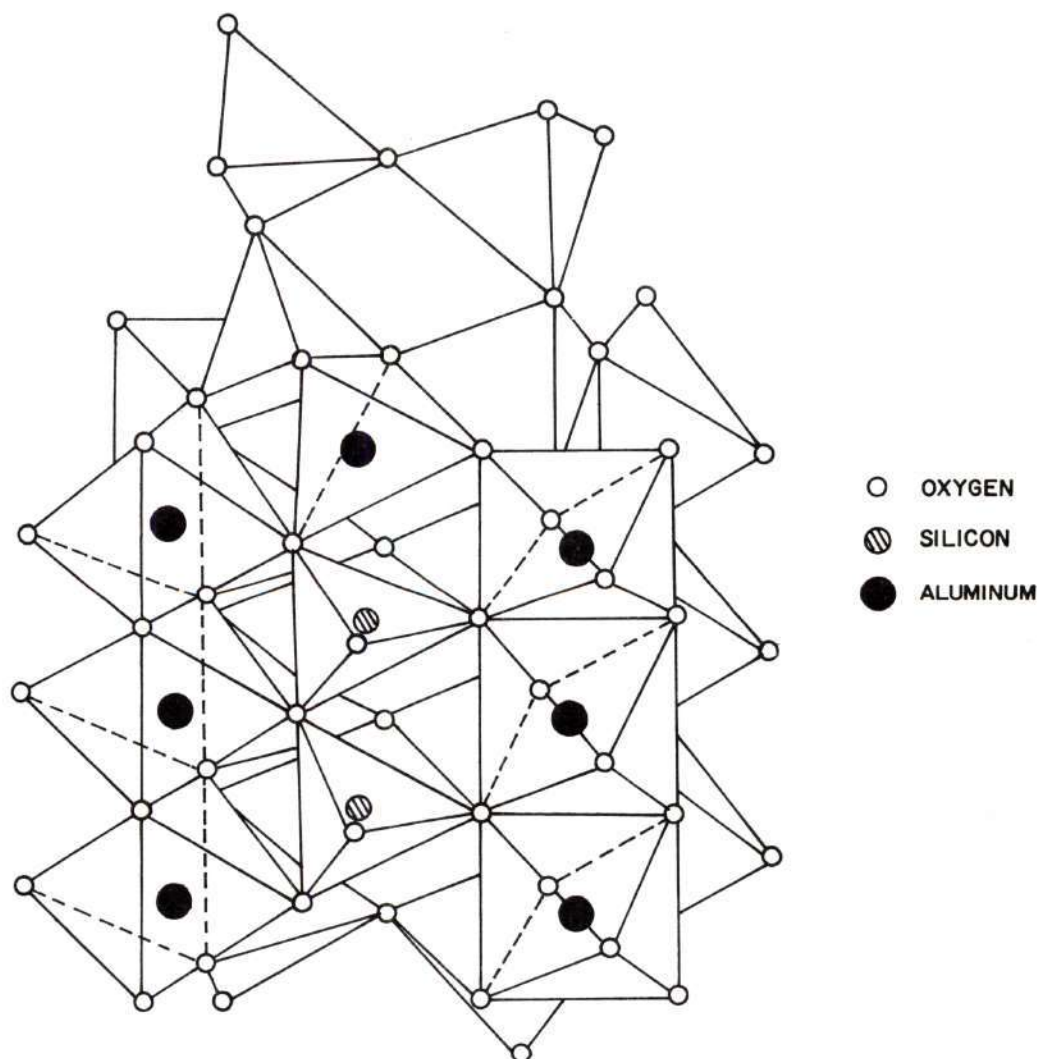
Mullite, the final stage in the kaolinite-mullite reaction series, forms as follows:



As reported by Brindley and Nakahira (9), the mullite structure is orthorhombic, with axial dimensions of $\underline{a} = 7.54 \text{ \AA}$, $\underline{b} = 7.69 \text{ \AA}$, $\underline{c} = 2.88 \text{ \AA}$. The alumina octahedra, linked together through edge-sharing, form chains parallel to the mullite \underline{c} axis. The alumina chains are aligned "parallel to the 110 axis of the spinel or parallel to the \underline{b} - axis of the original kaolinite" (10). The chains are bound together through lateral cross-linkage of alternating silica and alumina tetrahedra into three dimensional alignment with surrounding chains. For the present study the most important feature is that the alignment of the Al ions in the \underline{c} direction is carried forward from the kaolinite phase. The general alignment is row-like in mullite formed from well nb/3-crystallized kaolinite. Clays of poor nb/3-crystallinity show poor row formation due to nb/3 shifting (11).

The exact position of each ion in the mullite unit cell has not been accurately determined. The structure is known to be similar to that of sillimanite. However in mullite, half of the sillimanite silicon ions have been replaced with aluminum. At temperatures below 1400°C the structure is classed as a defect structure, due to the random positioning of excess silicon ions in interstitial sites of the mullite lattice. The mullite structure proposed by Durovic (12) is shown in Fig. 5.

The characteristics and extent of the mullite formation have been shown to be dependent upon several factors. Parmalee and Rodriguez (13) have shown that certain metallic ions (especially Fe, Zn, Mg, and Li) act as growth catalysts, while some alkali ions (principally Na and K) tend to hinder the transformation. Johns (14) indicates there is a relationship between the degree of mullite formation and the degree of "crystallinity"



ALUMINUM AND SILICON IONS ARE SHOWN ONLY IN
FRONTAL POLYHEDRA

Figure 5. Crystal Structure of Mullite.

of the kaolinite. Other investigators (15) indicate that the mullite crystal size is related to the kaolinite particle size, as might be expected if the mullite formation were essentially a surface phenomenon.

Mullite Preferred Orientation

Misalignment of the octahedral chains appears to have a pronounced effect on the degree of preferred orientation of the mullite crystals. Mullite growth, according to Comerfero, Fischer, and Bradley (16) appears to take place along Al_2O_3 octahedral chains possessing few random translations. Electron microscope studies by Comer indicate that preferred orientation may be somewhat related to "reaction product flow." He defines this term as "partial disintegration and loss of crystal boundaries in the 'reaction product' phase, presumably by diffusion" (17). Such flow is usually confined to small-sized, poorly nb/3-crystallized particles.

X-ray diffraction patterns generally do not indicate mullite orientation. This is probably because "mullite is oriented in three directions at 120° to each other, and in the relatively large volume examined with X-rays the mosaic character of the material gives a considerable angular spread to each of these directions" (18).

CHAPTER III

PROCEDURE

Three kaolinites of excellent, medium, and poor nb/3-crystallinity were irradiated by 0.667 mev gamma-rays. The effect of various radiation dosages on the nb/3-crystallinity of each was determined by X-ray diffraction.

Mullite growth kinetics of each kaolinite was studied with a high temperature X-ray diffractometer. Electron micrographs of fired samples were made to study mullite crystallite size and preferred orientation.

Specimen Characterization

Kaolinite Description

Samples of kaolinite of excellent, medium, and poor nb/3-crystallinity were obtained from Twiggs County, Georgia. Their descriptions are as follows: (1) "Georgia Kaolin," a raw, unprocessed clay (from Georgia Kaolin Company), with excellent nb/3-crystallinity, and 15 weight per cent of its particles less than 2 microns; (2) J. M. Huber Corporation's "Degrittied Crude" kaolinite, a clay of medium nb/3-crystallinity with 60 to 68 weight per cent of its particles less than 2 microns; and (3) "CWF" (produced by J. M. Huber Corporation), a poorly nb/3-crystallized filler clay, with 25 to 40 weight per cent of the particles less than 2 microns. The specific gravity of each clay was 2.6. Grain size distribution of each clay is shown in Appendix A.

Electrodialysis Process

The three kaolinite samples were electrodialyzed to replace exchange site cations (metal) with hydrogen ions. The clay to be dialyzed was made into a slurry containing 30 per cent clay by weight, and was placed in the sample section of the dialysis cell (Fig. 6). When the electric circuit to the cell was completed, ions moved through the solutions between the electrodes. Hydrogen ions produced by the water ionization replaced the metal cations on the clay particle surfaces. The metal cations migrated toward the cathode; solution anions moved toward the anode. The current flow in the system (shown by a milliammeter) indicated the degree of ion movement. The water in the electrode compartments was changed at frequent intervals, as high ion concentration about the electrodes tended to retard current flow. When the electric current had dropped to a minimum, the cation exchange was considered to have effectively ended. The replacement process is never complete, as some metal cations are tightly bound within the lattice.

The dried, dialyzed samples were screened through a U. S. No. 325 mesh screen. Samples of the screened and unscreened kaolinites were compared by standard optical emission spectrographic methods for their metal content. No increase in the metal content was observed due to screening.

Fluorescence Analysis

An X-ray Fluorescence Analysis was made of the impurity content of each kaolinite, using a General Electric XRD-5 D/F X-ray unit. A chromium target X-ray tube and a helium path were used for the determination of elements between $Z = 13$ (Al) and $Z = 22$ (Ti). Elements be-

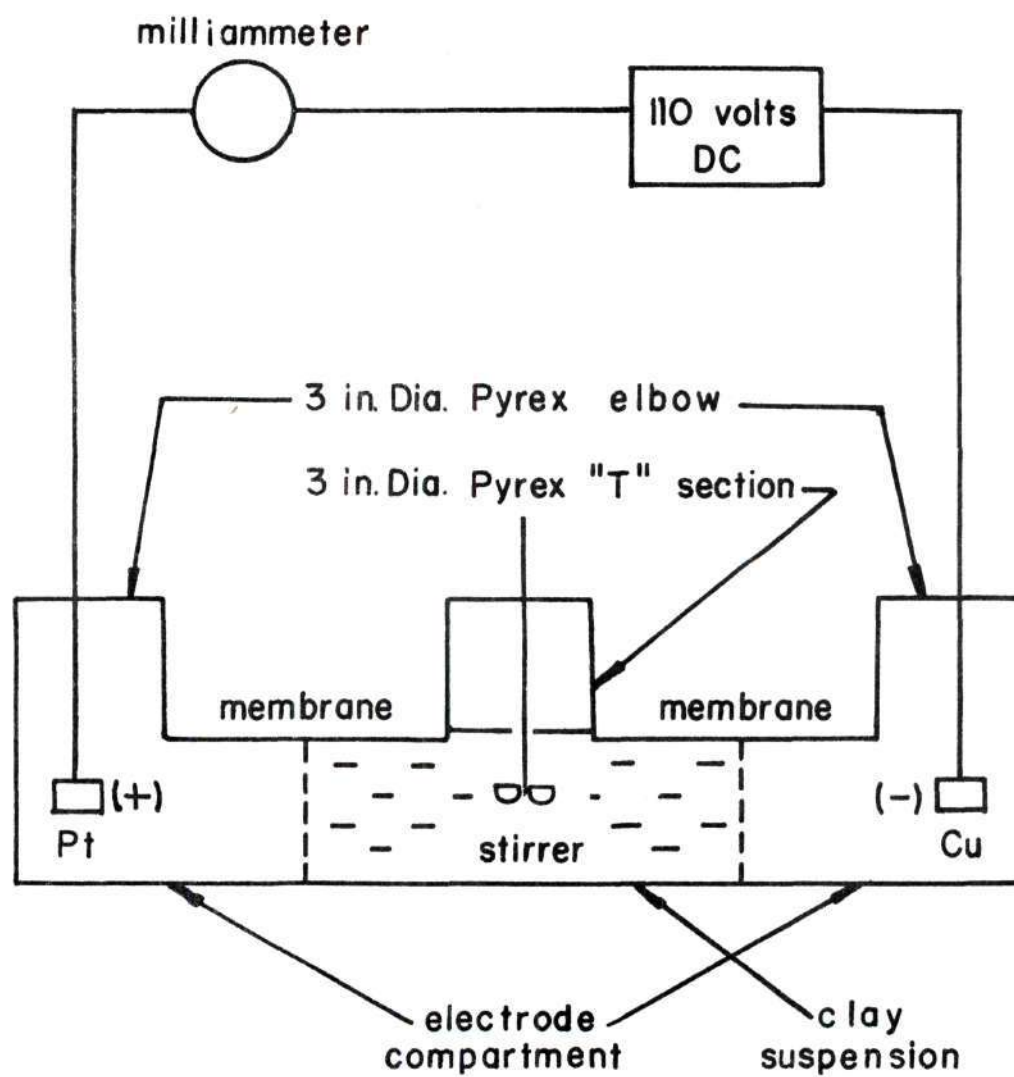


Figure 6. Electrodialysis Cell Schematic.

tween $Z = 22$ (Ti) and $Z = 56$ (Ba) were determined with a Pt target X-ray tube. Both EDT and LiF analysing crystals (with the faces cut parallel to the (200) plane) were used. Single wavelength fluorescent radiation was reflected from the crystal Bragg planes at angle θ , and was recorded by the counter at a corresponding 2θ value. Soller slits of 0.005 inches were used to eliminate divergent fluorescent radiation. A preliminary investigation was made using plexiglass in the sample carrier in order to determine the spectrum emitted by the tube alone.

To determine approximate impurity concentrations, the fluorescent intensities of the observed impurities were compared with similar fluorescence from prepared standards. The standards contained additions of the impurities observed (in the oxide form) in known increments. Five standards were prepared for each of the listed impurities (Table I) from a kaolin of known composition. The range of impurity additions varied from about 0.2 per cent to 1.0 per cent.

Table 1. X-Ray Fluorescence Analysis for Metal Impurities
(After Electrodialysis) in Kaolinite

Impurities	PER CENT PRESENT IN SAMPLE		
	Well nb/3- Crystallized	Medium nb/3- Crystallized	Poorly nb/3- Crystallized
Zr	0.2	0.2	0.25
Fe	0.7	0.9	0.8
Zn	0.05	0.1	0.15
K	None	Trace	Trace
Ti	1.1	1.25	1.0
TOTAL	2.05	2.45	2.20

Mineral Impurity Analysis

Nacrite, dickite, and montmorillonite are clay mineral impurities common in kaolin. The diffraction patterns of the three unirradiated kaolin were closely scrutinized for reflections which indicated the presence of these minerals. No nacrite, dickite, or montmorillonite was found.

The ethylene glycol test was also conducted for the presence of montmorillonite, as the presence of this mineral, even in amounts less than apparent from standard diffractometer techniques, would affect further test results. In this test the basal spacings (as indicated by a diffraction pattern) of an ethylene glycol saturated kaolin sample were compared with the spacings from an unsaturated sample. Ethylene glycol is readily absorbed into montmorillonite, where it expands the lattice, with correspondent shifting of the basal spacing. Such shifts would be apparent in the pattern, even if small amounts of montmorillonite were present. The test revealed no montmorillonite.

Gamma-Ray Irradiation

Samples of each kaolinite were irradiated with 0.67 mev gamma-rays. The radiation source was a Notre Dame type, Cesium-137 research irradiator, (rating-12,000 Curies) located on the campus of the Georgia Institute of Technology. A vertical intensity gradient existed in the center hole of the irradiator, with the exception of a three-inch long region with a constant dose rate of 7.5×10^{19} ev/gm/hr to ferrous ion dosimetry solution (the dosimeter solution was 0.01 N $(\text{FeNH}_4)_2(\text{SO}_3)$ and 0.8 N H_2SO_4 (19)).

A thin-walled aluminum container was constructed to hold a kao-

linite sample in the center hole region of constant dosage. The sample was packed with a bulk density of 0.66 gm/cc. The irradiation times and corresponding nominal dosages (assuming the absorption of the kaolinite to be the same as that of the dosimetry solution) are shown in Table 2.

Since the gamma-ray absorption of aluminum is relatively low, it was assumed that the aluminum holder did not affect the dosage absorbed by the kaolinite. Each sample was checked for radioactivity immediately upon removal from the irradiator. None was detected.

Table 2. Irradiation Dosages

Time in Irradiator	Nominal Dosage Received* (ev/gm/hr)
1 Minute	1.5×10^{18}
10 Minutes	1.5×10^{19}
100 Minutes	1.5×10^{20}
1000 Minutes	1.5×10^{21}
10,000 Minutes	1.5×10^{22}

* Assuming the absorption of kaolinite to be the same as that of a ferrous ion dosimeter solution. This assumption is probably valid within an order of magnitude.

Data Collection

nb/3-Crystallinity Determinations

X-Ray diffraction examinations with a Norelco diffractometer were made of each kaolinite sample. The nb/3-crystallinity index of each was

determined by the method of Johns and Murray (20). The index was expressed by the ratio of the $(02\bar{1})/(060)$ reflection intensities (expressed as integrated peak areas). The radiation effects on nb/3-crystallinity are shown in Table 3 and Fig. 7.

An attempt was made to detect any annealing effect due to irradiator temperature (60°C). Samples of unirradiated and 10^{19} ev irradiated medium and poorly nb/3-crystallized clays were heated to 60°C for 30 minutes. No change in the nb/3-crystallinity index was observed.

High Temperature Examinations

High temperature examinations were made to determine the quantities of mullite formed and the rates of mullite growth. Examinations were made with a high temperature attachment to the Norelco X-ray diffractometer unit, as diagrammed in Fig. 8.

The electric furnace of the unit was constructed from a 3.0 inch by 2.5 inch fused silica block, with seven 1.75 inch long, 22 gauge kanthal wire coils (0.25 inches in diameter) as heating elements. The kanthal coils were wound about zircon rods for support. Openings were made in each end of the furnace so that the furnace wall would not interfere with the passage of X-ray beams. The temperature was measured with a Pt-Pt(13%) Rh thermocouple nearly in contact with the X-rayed surface of the sample, and was controlled with a Wheelco 404 controller, or with manual operation of the autotransformer, or both. Since no color difference between the sample surface and the thermocouple junction could be observed with an optical pyrometer, the surface temperature differed from the thermocouple junction temperature by less than 10°C .

Table 3. nb/3-Crystallinity Index Determinations

Clay	Nominal Dosage	nb/3-Crystallinity Index
Georgia Kaolin	Unirradiated	0.56
(Well nb/3-Crystallized)	$1.5 \times 10^{18}\text{ev}$	0.57
	$1.5 \times 10^{19}\text{ev}$	0.61
	$1.5 \times 10^{20}\text{ev}$	0.55
	$1.5 \times 10^{21}\text{ev}$	0.53
	$1.5 \times 10^{22}\text{ev}$	0.53
Degrittred Crude	Unirradiated	0.29
(Medium nb/3-Crystallized)	$1.5 \times 10^{18}\text{ev}$	0.31
	$1.5 \times 10^{19}\text{ev}$	0.33
	$1.5 \times 10^{20}\text{ev}$	0.27
	$1.5 \times 10^{21}\text{ev}$	0.25
	$1.5 \times 10^{22}\text{ev}$	0.20
CWF	Unirradiated	0.24
(Poorly nb/3-Crystallized)	$1.5 \times 10^{18}\text{ev}$	0.26
	$1.5 \times 10^{19}\text{ev}$	0.28
	$1.5 \times 10^{20}\text{ev}$	0.28
	$1.5 \times 10^{21}\text{ev}$	0.22
	$1.5 \times 10^{22}\text{ev}$	0.19

The standard deviation of the nb/3-crystallinity index values shown was 5 per cent, as described in Appendix B.

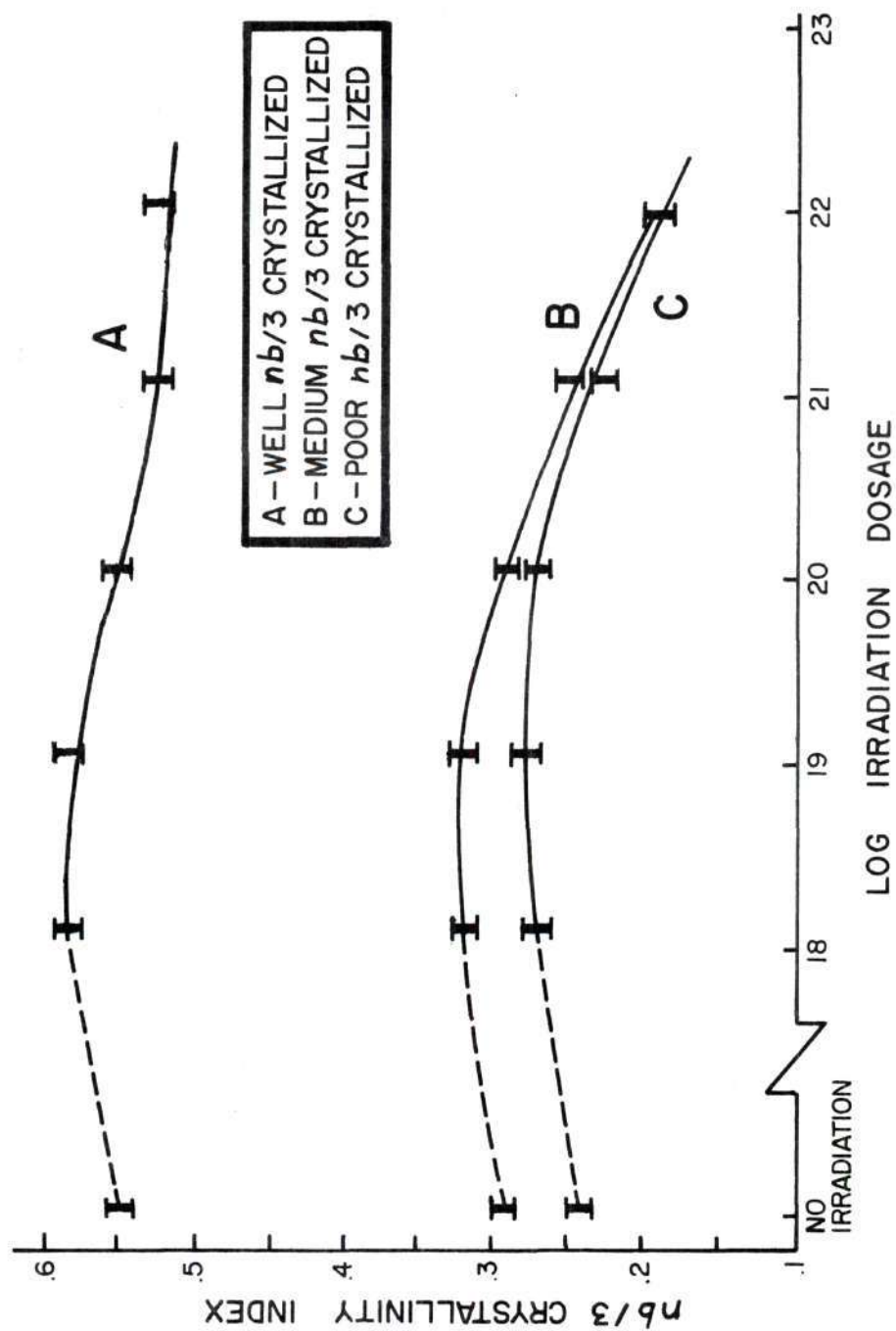


Figure 7. $nb/3$ -Crystallinity Changes by Irradiation.

The spread of the X-ray beam over a sample in the furnace was 1.3 cm. at $26.05^\circ 2\theta$ (the mullite reflection position). The furnace thermal gradient over this same area was approximately 8°C/cm as measured by an optical pyrometer. The controller attached to this furnace was consistently stabilized to within $\pm 10^\circ \text{C}$. The error in measuring the temperature differential between any two temperatures was approximately $\pm 5^\circ \text{C}$, as is shown in Appendix B.

Each kaolinite sample was packed loosely into a Pt dish. (Dense packing caused excessive sample buckling, from thermal expansion, which interfered with the X-ray beam). The sample holder was aligned horizontally on the center line between the Soller slits and the counter, and on the center line through the goniometer. To align the holder vertically, the counter was set at $0^\circ 2\theta$ and the X-ray tube voltage raised from minimum until a nearly full scale reflection was shown on the recorder. The sample was first raised vertically in the beam until the intensity dropped to one-half the full intensity. It was then "rocked" about the goniometer axis until the recorded intensity was maximized. The sample was then dropped out of the beam, and then raised vertically until the recorded intensity was exactly one-half the intensity when the sample was out of the beam. Thus the top surface of the sample was parallel to and at the same height as the X-ray beam center line. The final portions of this alignment procedure were repeated at temperature.

A further alignment check was made with the kaolinite (200) reflection. If the position of this reflection was altered or the intensity was not within what was considered a reasonable range, the sample

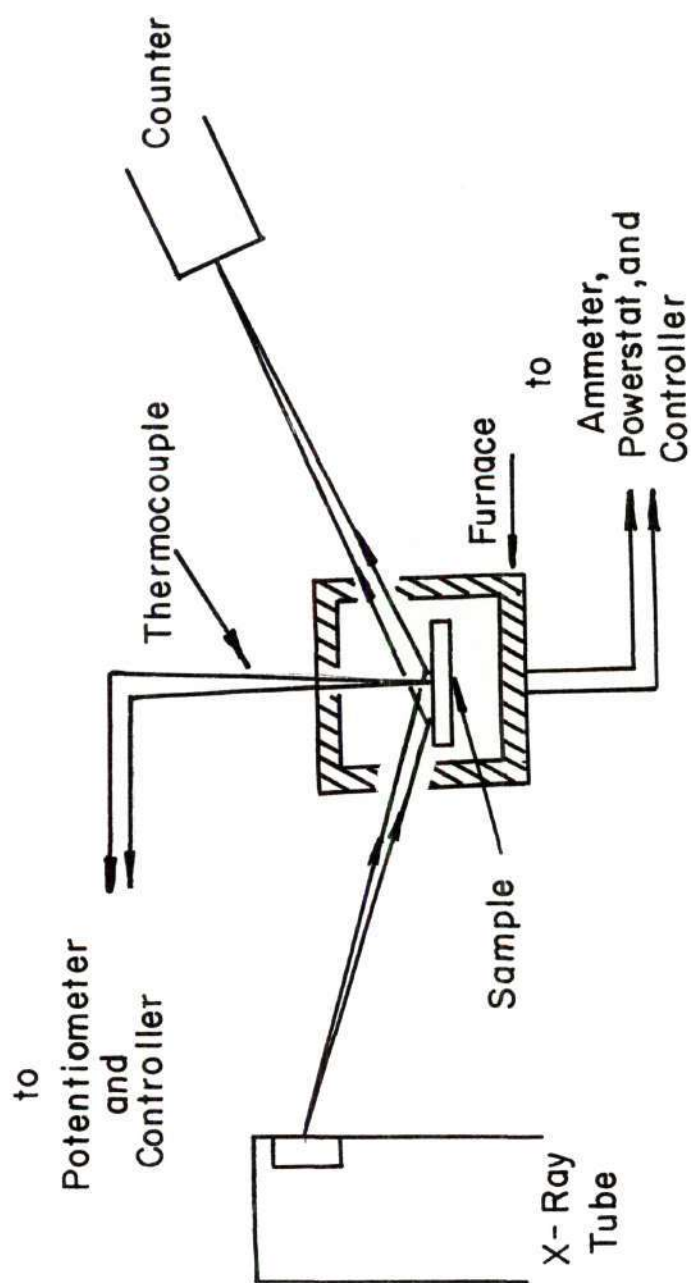


Figure 8. Schematic of High Temperature Diffraction Unit.

was assumed to be poorly aligned on the beam center line. In such cases the sample was realigned. The temperature of the sample was raised rapidly (within approximately ten minutes) from room temperature to the examination temperature. Three examination temperatures were used: 1100°C, 1150°C, and 1200°C. The proportional counter of the diffractometer oscillated with an angular range 2.5° (2θ) to either side of the mullite-sillimanite reflection pair. The main mullite reflection, the (210), occurred at 26.05° , the sillimanite reflection at 25.5° . The recorded diffraction patterns indicated the degree of mullite growth through reflection intensity changes. The growth was considered to have ended when no intensity increase of the mullite reflection was observed after 45 minutes to 1 hour from the time maximum intensity was reached.

When the high temperature examination was complete, the sample was cooled in place. The main mullite and sillimanite peaks were then rescanned to facilitate calculation of temperature effects on intensity for the particular sample.

The machine conditions were checked periodically. The X-ray tube current and voltage were reset prior to testing each specimen. The PHA (pulse height analyser) was reset at 90 per cent transmission before examination. The alignment was checked periodically by checking the 2θ position of reflections from a silicon standard. A fluorescent screen was used to check the centering of the X-ray beam. A standard intensity check was made daily of the silicon standard main reflection.

One irradiated clay was independently examined five times at each temperature for reproducibility determinations. The intensity variations were due to sample alignment, diffractometer operation, and particle

preferred orientation (minimized by careful packing). A deviation of 5 per cent was found in the early stages of firing and 3 per cent in the final stages (Appendix B).

Analytical Procedures

Reaction Product Growth

A sample of essentially 100 per cent mullite was obtained from the Norton Company for use as a standard in mullite formation calculations. The sample was ground and screened through a U. S. No. 325 mesh screen. A sample of cristobalite was similarly prepared. The samples were mixed in a mullite-cristobalite ratio of 63.6 per cent mullite to 36.4 per cent cristobalite by weight. This is the theoretical ratio at which mullite and cristobalite are produced by the kaolinite-mullite transformation.

An X-ray diffraction pattern was made of the standard before each high temperature examination. This produced an effective method of introducing a machine condition control into succeeding calculations.

The per cent mullite (at any time) in the sample was calculated from the diffraction patterns by the following equation:

$$M_t = (I_t/I_s)F \times 100\% \quad (5)$$

where M_t = Per cent mullite present at time t .

I_t = Integrated area of the sample reflection at time t .

I_s = Integrated area of the standard reflection (concurrently run).

F = Correction factor for temperature effect on intensity. This

factor is equal to the ratio A_c/A_f (where A_c = integrated area of the room temperature reflection, A_f = average integrated area of final mullite peaks--when growth is complete).

The percentages so obtained (Tables 4 through 6, Appendix C) actually reflect the amounts of mullite plus sillimanite present, as the reflection areas of the two overlapped in the basal portions of the X-ray pattern, and could not be resolved. The relative magnitude of the observed sillimanite and mullite peak areas (though unresolved) indicates that sillimanite is the predominant phase at 1100°C, and that mullite is the predominant phase at 1200°C. This effect is illustrated in Figure 9.

The sillimanite-mullite growth is shown graphically in Figures 10 A, B, and C. In the interest of clarity, not all of the experimental points are shown. The experimental values are presented in Tables 4-6 (Appendix C).

Mullite Activation Energy

Attempts were made to determine the mullite activation energy both by graphical methods and by computer programming of the decay product equation (third order). Both attempts were unsuccessful. Discussion of these methods is presented in Appendix D.

Mullite Crystallite Size and Microstrain

The width of the examined mullite reflection is due to several simultaneous causes, perhaps the most interesting of which are microstrain and crystallite size. (Microstrain is the term applied to strain which varies on a scale small compared to the particle size.) Diffraction peak broadening increases with strain. Diffraction peaks are also

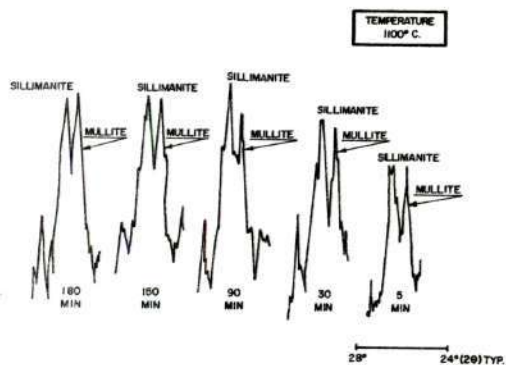
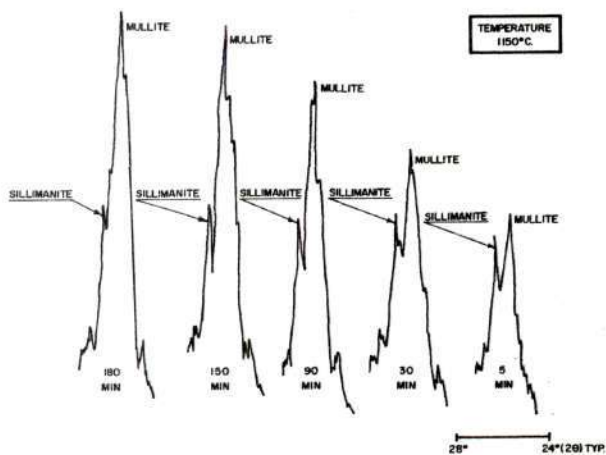
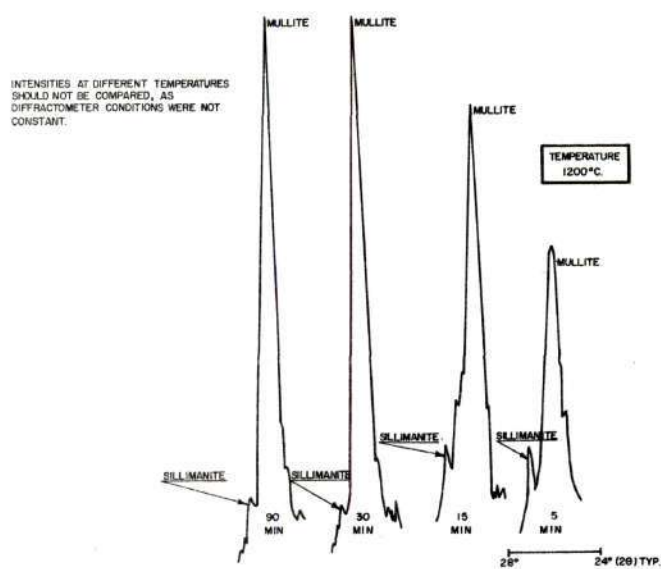


Figure 9. Diffraction Patterns of Sillimanite-Mullite Growth from Poorly nb/3-Crystallized Kaolin (10^{22} ev).

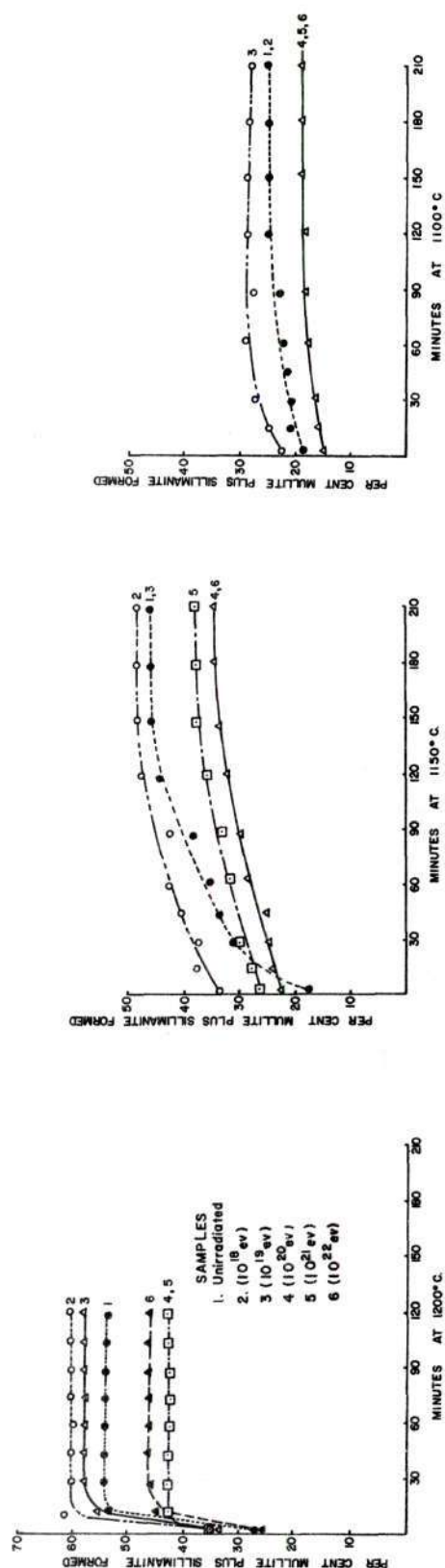


Figure 10a Sillimanite-Mullite Growth from Well
nb/3-Crystallized Kaolin.

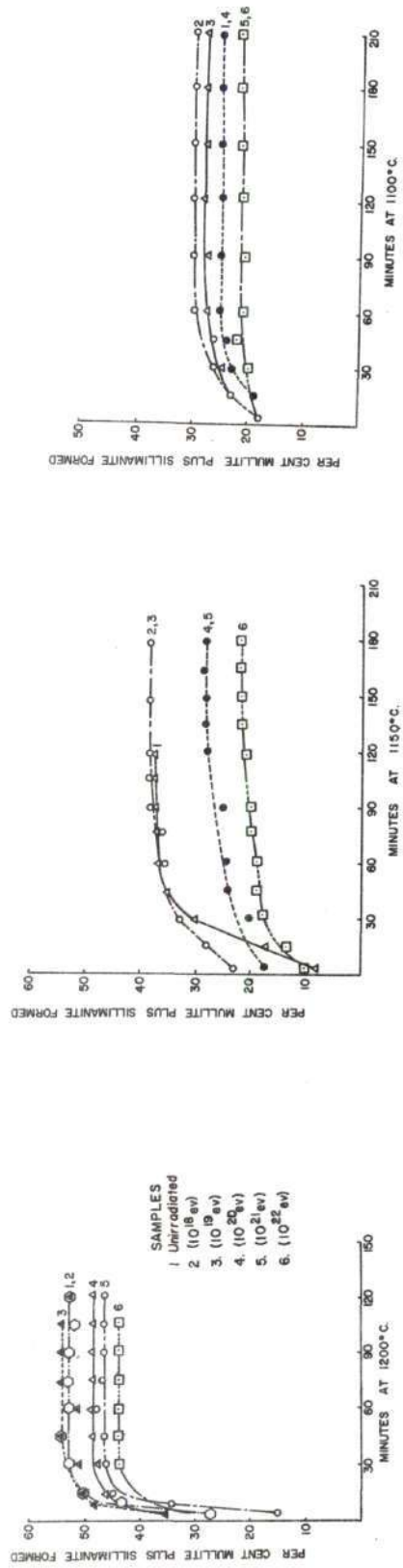


Figure 10b. Sillimanite-Mullite Growth from Medium
nb/3-Crystallized Kaolin.

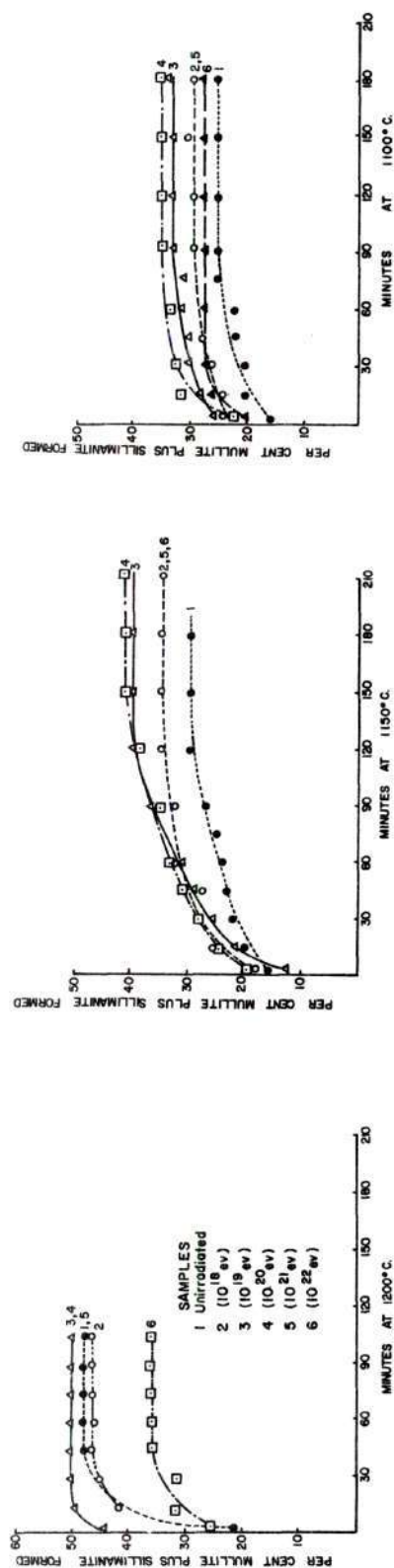


Figure 10c. Sillimanite-Mullite Growth from Poorly
nb/3-Crystallized Kaolin.

broadened if crystallite size is small enough to reduce the amount of destructive interference of the diffracted beams at angles near the exact Bragg angle. The breadth decreases as the crystal becomes larger (the number of parallel lattice planes in the crystal increases) due to a greater tendency for complete interference at angles near the Bragg angles.

Measurements of the integrated resolved (estimated) mullite peak breadth were made of each sample. The average integral breadth of the observed peaks was $1.8^\circ(2\theta)$. The breadth decreased approximately $0.1^\circ(2\theta)$ as time increased to the point of approximately constant growth rate. There was a generally consistent decrease in the breadth of approximately $0.05^\circ 2\theta$ as the temperature was raised from 1100°C to 1200°C for all radiation doses. The standard deviation of the breadth measurements were 5 per cent as discussed in Appendix B. Thus the change in breadth was within the range of experimental error in breadth determination. If real, these breadth changes indicated possible strain relief, increase in crystallite size, or combinations of both.

Electron Microscopy

Samples of each kaolinite were heated during a 20-hour cycle to 1200°C in a 1500 watt Paragon kiln (model T-7).

The fired samples were examined by an electron microscope, utilizing standard preshadowed platinum replica techniques. The presence of mullite in these samples was indicated by X-ray diffraction.

The particle surfaces in Figs. 11A and B (poorly nb/3-crystallized kaolinite--unirradiated and 10^{19}ev , respectively) show some deformation of the particle edges and the presence of rounded nodules, which are pre-

sumed to be mullite in the initial formation stages. The nodules of the unirradiated sample are larger, but in less abundance than those of the low dosage irradiated one. The detail of Fig. 11C is insufficient to reveal any reaction products. The specimens of Fig. 12 (medium nb/3-crystallized kaolinite) show larger, more well-defined needles than those of the previous figure, and greater boundary decay (particularly in Fig. 12 A and B). The needles are seen in random orientation. The micrograph features of the well nb/3-crystallized sample of Fig. 13 are essentially the same as those of Fig. 12. No quantitative results were deduced from the micrographs because of a lack of reproducibility. However, they do not disagree with X-ray diffraction results.

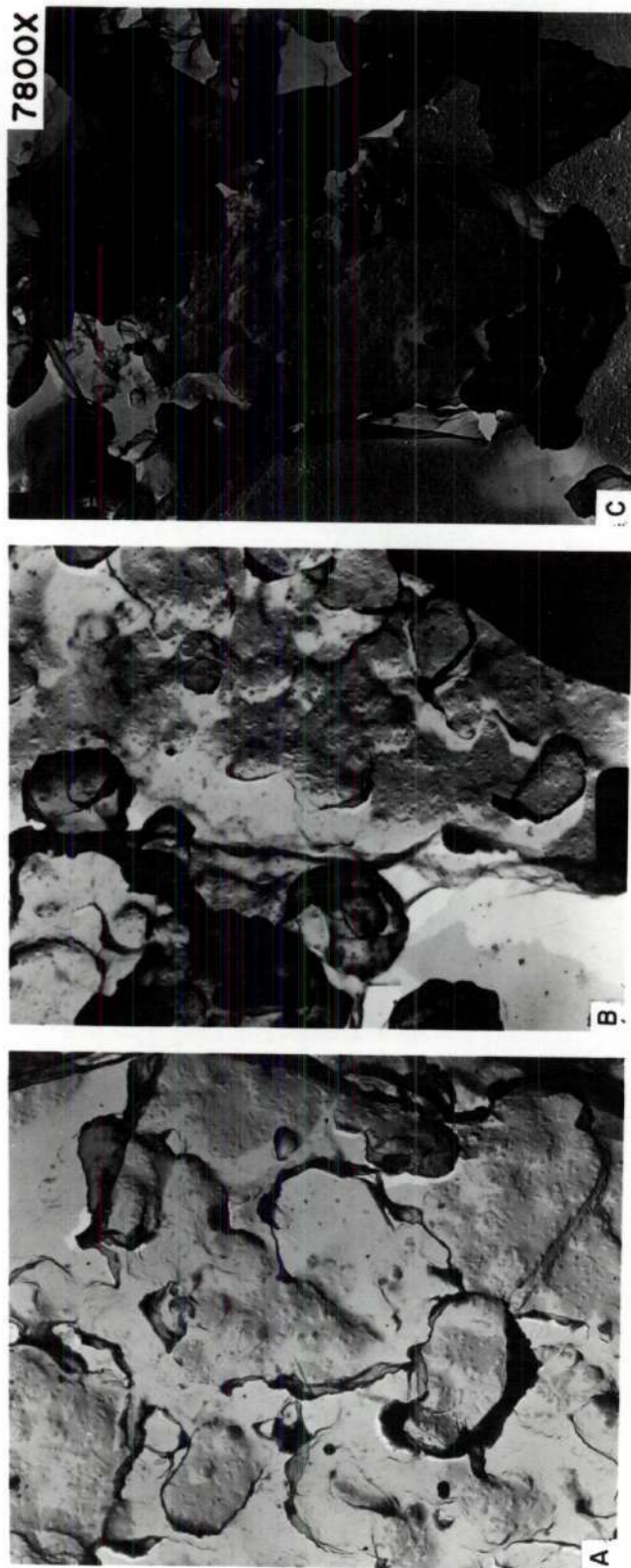


Figure 13. Electron Microscope Studies of Mullite Growth from Well nb/3-Crystallized Kaolin.

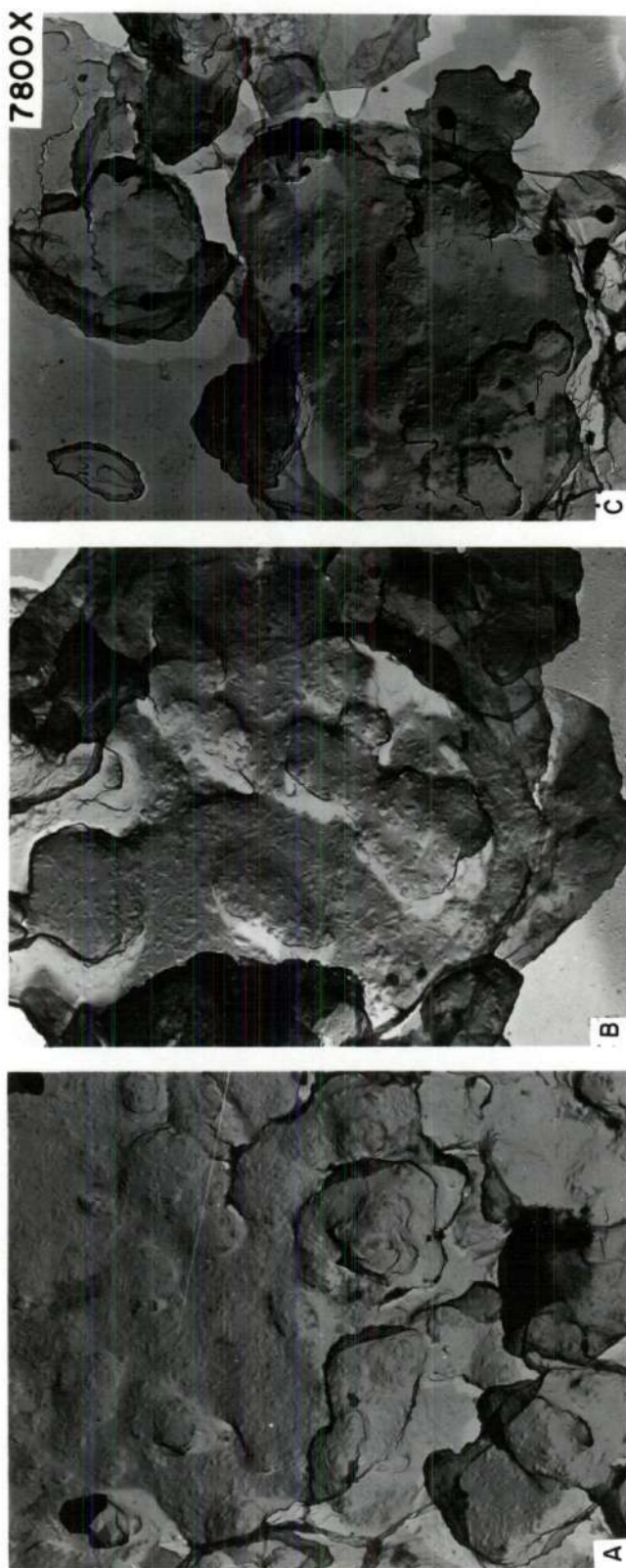


Figure 12. Electron Microscope Studies of Mullite Growth from Medium nb/3-Crystallized Kaolin.

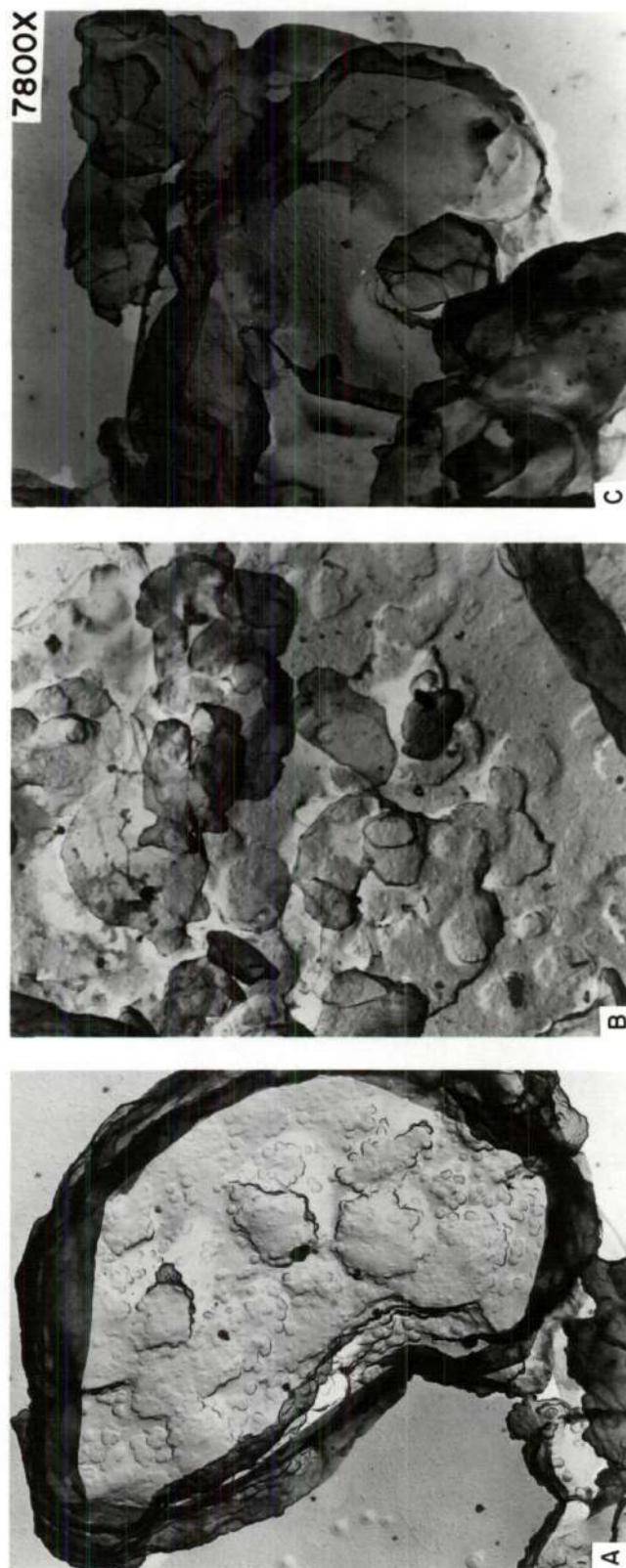


Figure 11. Electron Microscope Studies of Mullite Growth from Poorly nb/3-Crystallized Kaolin.

CHAPTER IV

DISCUSSION OF RESULTS

Kaolinite Radiation Damagenb/3-Crystallinity Variations

Exposure of kaolinite to 0.67 mev gamma-rays produced observable radiation damage. The nb/3-crystallinity of the three kaolinite samples apparently improved for radiation doses through approximately 10^{19} ev/gm (at which time the crystallinity index reached a maximum value), and declined progressively for larger doses. The changes are shown in Fig. 7 and Table 3. Investigations of the (002)/(060) ratio of the reflection intensities indicated that the apparent nb/3-crystallinity increase was not caused by Gitterstörung (static ion displacement) reduction of the (060) reflection intensity. A considerable portion of the nb/3-crystallinity improvement lay within the range of experimental error (5 per cent, Appendix B).

nb/3-Crystallinity improvement might be produced by either, or both, of the following mechanisms: (a) migration of impurity ions located in substitutional or interstitial positions, and (b) radiation annealing of crystal disorders which existed prior to irradiation (21). These suppositions would also account for the fact that the poorly nb/3-crystallized clays showed the greater improvement in their crystallinity index, as would be expected from clays containing more impurities or disorders.

The crystallinity improvement was probably real, as both the amount of reaction products formed and the relative growth rates varied in direct relation to the observed crystallinity.

X-ray fluorescence analysis showed no change in the impurity content due to irradiation. This does not mean, however, that the gamma-rays did not cause impurity migration.

Damage Mechanisms

Two possible damaging mechanisms that may result in alteration of the crystallinity index include nb/3 shifting of the individual sheets and random movement of the Al ions among the possible Al sites in the lattice. The random Al ion movement is more likely because of the lower energy requirement for the movement of the small Al ions (0.50 \AA radius), and the general nature of the Al lattice sites (only two-thirds filled).

The methods utilized in this work do not give sufficient evidence to distinguish between the two mechanisms. The probable mechanism, however, proceeds as described below.

As gamma-rays pass through a kaolinite crystal they interact with the atomic electrons to produce Compton electrons. The Compton electrons are of sufficient energy to displace ions indiscriminately (chiefly Si and Al due to their small size and atomic number) upon collision. The displaced ions would tend to settle in energetically stable positions. Such positions would include their original sites, similar vacant sites, substitutional sites, or some interstitial sites. The Al ions have little trouble in finding a stable site, since their possible sites are only two-thirds filled initially. A few silicon ions may move into Al sites, though this is unlikely, as the respective sites are in different

layers.

It is expected that the Si displacements anneal much more rapidly than do those of the Al. This is because the Al ions are generally stable in any of their possible sites, one-third of which are different from their initial ones. Thus, diffraction examinations for radiation damage show principally the effect of the Al ion displacement or, in effect, nb/3-crystallinity index variations (as shown in Figs. 3 and 4). This also accounts for the fact that no nb/3-crystallinity improvement was noted for samples annealed at 60°C.

A careful differential thermal analysis using an unirradiated kaolinite standard versus irradiated kaolinite might help distinguish between the damaging mechanisms.

Mullite Formation Kinetics

General Considerations

The formation of mullite from kaolinite is probably not a simple exponential function in its early stages, though such is superficially suggested from the curves of Fig. 10. Plots (not shown) of log M (amount remaining to be reacted) vs. t (time at temperature) did not result in straight lines as would have been the case had mullite growth been a simple process. In view of the number of phase transformations involved, the non-linearity of the log M vs. t plots was to be expected. It was this non-linearity which suggested the use of a computer for determination of the growth constants. It may be possible to determine activation energy of mullite formation from plots of log M vs. log t, though such was not attempted.

nb/3-Crystallinity Effect on Mullite Formation

The use of gamma-radiation provides a particularly attractive method for determining the effect of kaolinite "crystallinity" on mullite formation, because it permits the elimination of essentially all of the variables except nb/3-crystallinity.*

The following changes in mullite growth were common to the three types of kaolinite: (1) the slight increases in the amount and rate of mullite growth with apparent improvement of the nb/3-crystallinity index for irradiation dosages less than 10^{19} ev/gm, and (2) the decrease in amount and rate of mullite growth accompanied by the decrease in nb/3-crystallinity index for irradiation doses greater than approximately 10^{19} ev/gm. These effects are shown in Fig. 10 A, B, and C.

Correlation of these results with Brindley, Nakahira (22), and Comer (23) indicates that the preferred mullite growth mechanism involves an energetically favored relationship, based on the orderly preservation of alumina chains throughout the phases succeeding kaolinite. In the absence of such a relationship, one might expect the poorly crystallized material to transform most readily, as the free energy of the disturbed lattice would be expected to be larger than that of the undisturbed lattice.

The orientation information appears to be propagated from the initial kaolinite crystals in an epitaxial relationship through three intermediate phases (metakaolin, spinel phase, and sillimanite) to the

* The other variables are held effectively constant with the exception of particle size which may become significant for the highest radiation doses.

mullite phase. The transformation is probably in accordance with the Brindley-Nakahira mechanism (24), which is based on maintenance of an orderly arrangement of alumina octahedra throughout the several phase transformations. For this model additional thermal energy would be required to allow the disarranged alumina octahedra to re-order in the mullite phase positions, an order they would have had anyway if the original kaolinite had not been disordered. The observed correlation of mullite formation with nb/3-crystallinity index (within a series of samples of a given clay) is therefore explained by the Brindley-Nakahira mechanism.

Comer (25) has strongly corroborated the Brindley-Nakahira mechanism by showing that the spinel phase is preferentially oriented in the manner predicted by this mechanism. Comer also notes that the spinel phase crystallite sizes all seemed to be in the range 75 \AA to 125 \AA . Comer's electron micrograph studies (26) of preferred mullite growth (from kaolinite of varying crystallinity) indicate that mullite orientation is associated with the ordered positions of the Al ions. Preferred mullite growth from a well nb/3-crystallized kaolinite occurred in three directions (120° apart), as would be expected if the Al ions were properly located in their pseudo-hexagonal positions. Reduced nb/3-crystallinity appeared to hinder the mullite chain formation, resulting in random directional growth.

The electron micrographs (Fig. 11-13) showed little if any mullite preferred orientation. However, they do support the suggestion of an epitaxial mechanism, as less or no mullite was seen on the samples of the poorly nb/3-crystallized kaolinite.

Effects of Variables

Behavioral differences among the three clays may be related primarily to the nature of the clay impurities and to the manner of their incorporation. It is presumed that the larger content of catalytic iron (27) of the "medium crystallized" kaolinite caused this clay to yield more mullite (in some cases) than did the "well crystallized" kaolin. Such would be predicted if the iron were to enter preferentially at the "nearly equivalent" and ideally vacant Al sites in the crystal. This specially placed iron would both enhance the (060) and diminish the (021) intensities, effectively lowering the nb/3-crystallinity index. By its presence, the iron might be expected to add to the lattice energy, thus helping to activate nucleation centers without having any particular effect toward raising the activation energy of any of them.

Other differences in behavior may be attributed to grain size distribution (Appendix A) and to crystal imperfections other than nb/3-crystallinity. The latter are implied by possible preferential reduction of the (060) intensity by general lattice distortion and observed changes (slight) in the ratio of the (001)/(002) reflection intensities, which indicate ionic rearrangement.

The results suggest that two competing radiation damage effects require identification: (1) energy stored in the lattice is available to enhance nucleation and growth, and (2) the formation of particular point defects, especially those consisting of movement of the Al ions into nearly equivalent sites, disrupts the orderly arrangement of alumina octahedra and thereby inhibits mullite formation.

It has not been established here whether the nb/3 shifting of

Al ions (presumed measured by the nb/3-crystallinity index) is actually the most important process of nucleation-center destruction or merely correlates with it. In either event, it would be expected that the number of nuclei of "normal activation energy" would decrease with increasing radiation and that the observed correlations of inhibited mullite formation and decreased nb/3-crystallinity with heavy irradiation, and with each other, would be found.

Since the differences among the various mullite formation curves occur in the first few minutes "at temperature," it appears that the differences brought about either by irradiation or by initial nb/3-crystallinity variations are primarily differences in nucleation. This would be expected if the number of nucleation centers are not materially affected by low radiation dosages and that the additional lattice energy thereby provided more than compensates for any reduction in the number of centers.

Silica Growth

Silica is a by-product of the kaolinite-mullite transformation. The silica crystallizes initially as tridymite, but converts to cristobalite with prolonged heating (above 925°C). The observed tridymite peak was broad, relatively low in intensity, and increased little with time. There were some indications of its conversion to cristobalite, though the main X-ray reflection was very diffuse and poorly defined. Measurements of the extent and character of the silica liberation were limited to a small number of samples and discontinued because of the lack of well-defined peaks for analysis.

CHAPTER V

CONCLUSIONS

1. Exposure of kaolinite to 0.67 mev gamma-rays induces observable changes in the nb/3-crystallinity index. Radiation doses less than about 10^{19} ev/gm apparently improve the nb/3-crystallinity; radiation damage from higher doses lowers the nb/3-crystallinity.

2. The nature of the radiation damage is two-fold: (1) disruption of the row of Al ions, shown by nb/3-crystallinity changes, and (2) general increase in the lattice energy, presumably by formation of point defects involving all kinds of atoms present.

3. The irradiation method of inducing nb/3-crystallinity changes allowed a clear demonstration of the direct dependence of mullite formation kinetics on nb/3-crystallinity. This is unambiguously shown because the other variables affecting mullite growth are not affected by the irradiation changes.

4. Light irradiation (up to about 10^{19} ev/gm as measured by ferrous ion dosimetry) probably enhances mullite formation in most cases, and never inhibits it.

5. Heavy irradiation (doses greater than about 10^{19} ev/gm) inhibits mullite formation.

6. The decrease in both the mullite reaction rate and the quantity formed with decreasing nb/3-crystallinity or increased disordering of the Al ions provides strong evidence that an epitaxial growth of mullite, based on ordered alumina chains, is energetically favored to a substantial degree.

APPENDIX A

GRAIN SIZE DISTRIBUTION OF KAOLINITE SPECIMENS

The grain size distribution of the original kaolinite samples was determined with the aid of a Coulter counter (Coulter Industrial Sales, Chicago, Illinois), by Messrs. W. J. Corbett and J. H. Burson of the Chemical Engineering Department, Georgia Institute of Technology. This device determined the quantity of various particle sizes suspended in an electrically conductive fluid. Test results are shown graphically in the accompanying figure.

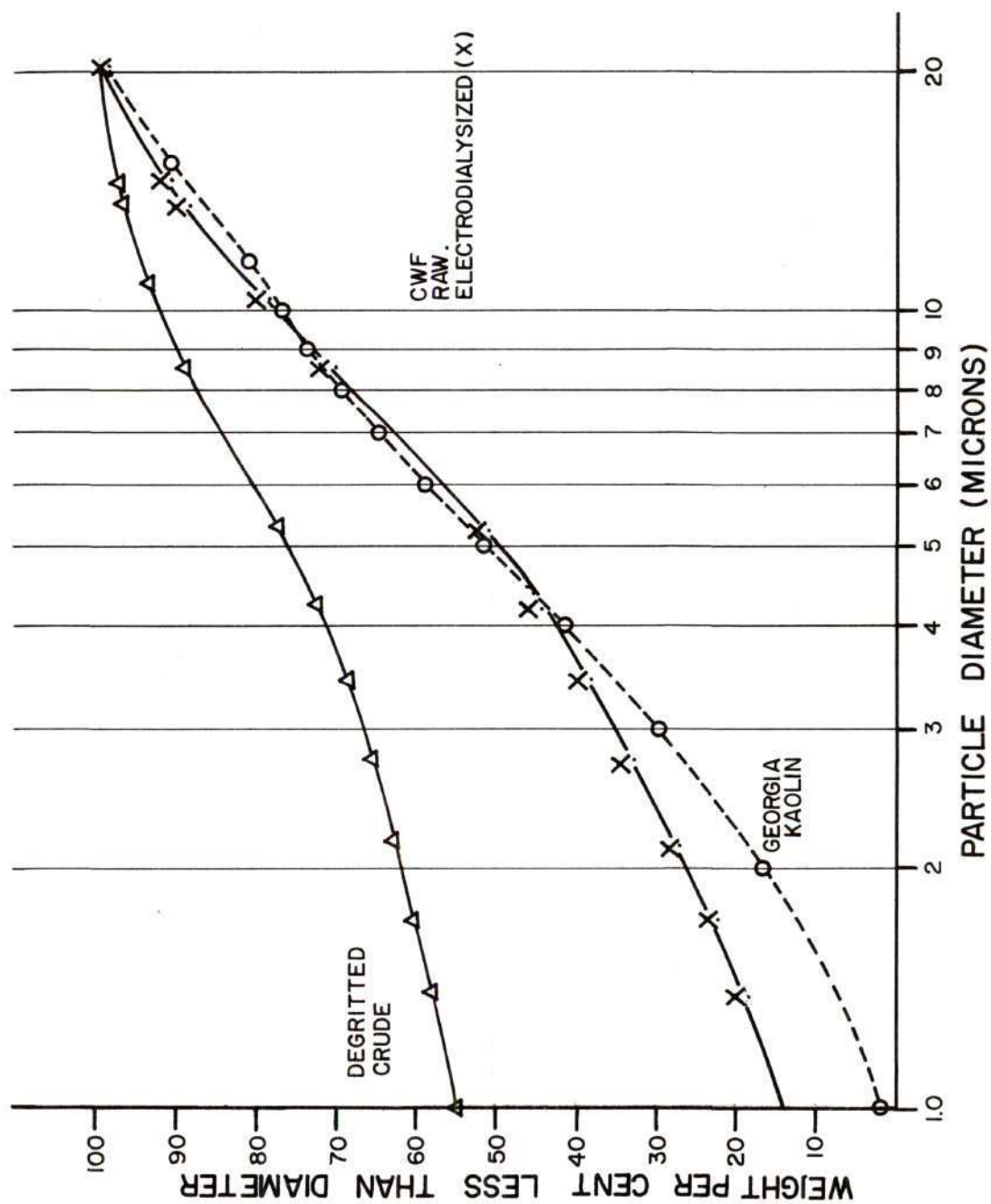


Figure 14. Particle Size Distribution of Sample Clays.

APPENDIX B

CALCULATION OF ERRORS

General Error Determinations

An important feature of this investigation is a knowledge of the errors involved. Such errors are usually expressed in per cent standard deviation (σ), which is calculated as follows:

$$\sigma = \sqrt{\sum \frac{(x-\bar{x})^2}{N-1}} \times \frac{100\%}{\bar{x}} \quad (6)$$

where x = Observed or calculated value of M_t or Crystallinity Index

\bar{x} = Mean value of M_t and/or Crystallinity Index.

N = Number of samples examined.

M_t = Per cent mullite present at time t (eq. 5)

In the case of the crystallinity determinations is based on the reproducibility in the $(02\bar{1})/(060)$ measurements from seven unirradiated Degritt Crude samples under conditions previously described, plus measurements from three samples of each of the other unirradiated clays ($N = 13$). The value of σ was found to be 5 per cent.

Mullite growth was reproduced in independent experiments for five samples of a given kaolin at each temperature. From these samples the standard deviation of the mullite content was calculated for each temperature from equation (6). Deviation values are shown in Tables 4D, 5D, and 6D. The average deviation (for the three temperatures involved) was 5 per cent in the early stages of firing and 3 per cent in the final stages.

Because complete and independent heating experiments were performed, these σ values included errors due to sample packing, heating, and alignment in the X-ray beam. The standard deviation of the peak breadths was obtained from the same investigation, and was found to be 5 per cent.

Temperature Measurement Errors

The errors of precision (as opposed to accuracy) in the temperatures were due to the following causes: (1) placement of the thermocouple with respect to the sample, (2) change in the thermocouple calibration with time at temperature, (3) inaccuracies in reading the potentiometer, and (4) errors in reading the thermocouple emf.

The temperature was observed for a small area occupying the center of the sample. Small displacements of the thermocouple from the ideal position above the sample center gave different temperature measurements for this area. Such displacements, coupled with the same thermal gradient ($8^{\circ}\text{C}/\text{cm}$) gave a maximum error of $\pm 10^{\circ}\text{C}$. However, the actual error was probably less.

Prolonged exposure of the thermocouple to high temperatures may have altered the calibration of the thermocouple slightly. New thermocouples were installed and calibrated after approximately 50 hours usage to remedy any such changes.

APPENDIX C

MULLITE GROWTH DATA

The following data were collected from high temperature X-ray diffractometer examinations.

An explanation of the symbols used is as follows:

I_t = Integrated intensity of sample mullite reflection at time t .

Units = $\text{in}^2 \times 100$

M_t = Per cent mullite present at time t (see page 24).

Mullite Standard Intensity is the integrated intensity of the (210) reflection of the "pure" mullite sample used as a standard. This intensity was determined concurrently with each specimen evaluation.

Units = $\text{in}^2 \times 100$

Final Peak Intensity is the integrated intensity of final reflection, observed after sample had cooled to room temperature.

Peak Height is measured in inches.

B_0 = $(I_t/\text{peak height}) \times .005^\circ(2\theta)$ per inch, and is the integral breadth in degrees 2θ .

Table 4. Mullite Growth--1200°C

A. Well nb/3-Crystallized Kaolin

Unirradiated		Mullite Standard Intensity														Final Peak Intensity	
Time (min.)		2	4.5	9	11	16	31	46	61	76	91	106	121				
It	74	134	142	145	146	146	148	146	146	146	146	152	148			305	164
Mt	27.4	49.3	52.0	53.5	53.5	54.8	54.8	54.0	54.0	54.0	54.0	56.2	54.8				54.0
Peak Height	3.0	5.4	6.3	6.2	6.4	6.5	6.5	6.5	6.6	6.8	7.2	6.9	7.0				7.8
Bo	1.23	1.28	1.12	1.17	1.13	1.13	1.13	1.12	1.11	1.08	1.01	1.10	1.06				1.04
<hr/>																	
10 ¹⁸ ev/gm		Mullite Standard Intensity														Final Peak Intensity	
Time (min.)		1	3	8	10	15	30	45	60	75	90						
It	82	90	115	130	132	137	137	137	140	139	138					257	155
Mt	35.6	39.0	51.2	56.4	61.0	59.6	59.6	59.6	61.0	60.4	60.2						60.4
Peak Height	2.3	3.3	4.2	4.5	5.3	6.1	6.1	6.0	6.0	6.2	5.8						7.0
Bo	1.78	1.36	1.37	1.45	1.24	1.12	1.12	1.13	1.16	1.12	1.19						1.10
<hr/>																	
10 ¹⁹ ev/gm		Mullite Standard Intensity														Final Peak Intensity	
Time (min.)		1	3	8	10	15	30	45	60	75	90						
It	80	112	130	133	135	140	140	140	140	140	138					257	148
Mt	33.0	46.0	53.6	54.8	55.8	58.0	58.0	58.0	58.0	58.0	56.8						57.8
Peak Height	3.3	4.0	5.0	5.2	5.4	6.1	6.1	6.3	6.1	6.3	6.4						6.8
Bo	1.21	1.40	1.30	1.31	1.26	1.15	1.15	1.11	1.15	1.11	1.07						1.09
<hr/>																	
10 ²⁰ ev/gm		Mullite Standard Intensity														Final Peak Intensity	
Time (min.)		1	3	8	10	15	30	45	60	74	89						
It	92	107	110	110	110	110	110	110	110	110	110					282	120
Mt	35.6	41.4	42.6	42.6	42.6	42.6	42.6	42.6	42.6	42.6	42.6						42.6
Peak Height	3.8	4.5	4.5	5.1	5.0	4.7	4.7	4.6	4.8	4.7	4.7						5.2
Bo	1.18	1.19	1.22	1.10	1.10	1.10	1.17	1.17	1.12	1.12	1.13						1.15
<hr/>																	
10 ²¹ ev/gm		Mullite Standard Intensity														Final Peak Intensity	
Time (min.)		1	3	8	10	15	30	45	60	75	90						
It	82	100	106	110	110	110	108	109	112	107	107					282	120
Mt	32.0	39.0	41.2	43.0	43.0	42.2	42.2	42.4	43.6	41.8	41.8						42.6
Peak Height	3.3	4.0	4.4	4.7	4.6	4.7	4.7	4.9	5.2	5.1	4.8						6.0
Bo	1.24	1.25	1.32	1.15	1.19	1.18	1.18	1.11	1.10	1.04	1.13						1.00
<hr/>																	
10 ²² ev/gm		Mullite Standard Intensity														Final Peak Intensity	
Time (min.)		2	4.5	9	11	16	31	46	61	76	91						
It	75	91	110	121	121	121	123	123	122	122	124					308	140
Mt	27.4	33.4	40.4	44.4	44.4	44.4	45.2	45.2	45.2	44.8	45.6						44.8
Peak Height	2.3	3.3	4.0	4.7	4.8	5.6	5.6	5.6	5.5	5.5	5.6						7.4
Bo	1.64	1.38	1.38	1.27	1.25	1.10	1.10	1.10	1.11	1.11	1.11						1.10

* Explanation of table captions appears on page 47.

Table 4. Mullite Growth--1200°C (Continued)

B. Medium nb/3-Crystallized Kaolin*

Unirradiated		Mullite										Final
Time (min.)		Standard Intensity										Peak Intensity
2		4.5	9	14	29	44	59	74	89	104	119	-
67		100	105	123	128	130	128	127	126	122	128	138
It		27.6	41.2	43.4	50.8	52.8	53.6	52.8	52.0	50.4	52.8	52.6
Peak Height		2.2	4.2	4.8	5.1	5.5	5.8	5.2	5.6	5.3	5.3	6.1
Bo		1.54	1.19	1.19	1.20	1.15	1.11	1.22	1.12	1.15	1.20	1.12
10 ¹⁸ ev/gm												
Time (min.)		4.5	9	11	16	31	46	61	76	91	106	-
80		99	106	113	115	117	114	117	113	115	115	133
It		36.0	44.4	47.6	50.8	51.8	52.6	52.6	50.8	51.8	51.8	51.6
Peak Height		3.2	4.4	4.9	5.4	5.5	5.8	4.9	4.9	5.2	5.2	7.3
Bo		1.25	1.12	1.08	1.04	1.01	1.15	1.16	1.14	1.11	1.11	0.91
10 ¹⁹ ev/gm												
Time (min.)		4.5	9	11	16	31	46	61	76	91	106	-
82		100	113	116	118	124	120	123	123	120	120	140
It		35.4	43.3	48.6	50.2	50.8	51.6	53.0	53.0	51.6	51.6	51.5
Peak Height		3.4	4.8	5.3	5.4	5.8	5.6	5.7	5.8	5.2	5.6	6.4
Bo		1.28	1.03	1.22	1.16	1.08	1.04	1.07	1.06	1.15	1.10	1.10
10 ²⁰ ev/gm												
Time (min.)		3	8	10	15	30	45	60	75	83		-
103		112	122	125	130	134	130	133	133	133		135
It		37.8	41.2	44.8	46.0	47.4	47.4	47.8	48.8	48.8		48.0
Peak Height		4.6	4.7	5.0	5.0	5.2	4.8	4.9	4.7	4.8		4.8
Bo		1.20	1.21	1.20	1.25	1.28	1.32	1.35	1.35	1.38		1.40
10 ²¹ ev/gm												
Time (min.)		4.5	9	11	16	31	46	61	76			-
43		70	92	120	123	128	127	130	128			130
It		16	26.0	34.2	44.4	45.6	47.0	48	47.4			47.6
Peak Height		1.4	2.4	4.0	4.7	5.0	5.1	5.8	5.6			6.6
Bo		1.54	1.45	1.15	1.25	1.23	1.08	1.09	1.13			0.98
10 ²² ev/gm												
Time (min.)		4.5	9	14	29	44	59	74				-
54		80	95	97	100	101	100	100				120
It		24.0	35.6	41.6	42.8	44.0	44.6	44.0				44.0
Peak Height		1.6	2.8	3.2	3.8	4.0	4.4	4.3				5.2
Bo		1.68	1.43	1.48	1.26	1.25	1.13	1.16				1.18

* Explanation of table captions appears on page 47.

Table 4. Mullite Growth--1200°C (Continued)

C. Poorly nb/3-Crystallized Kaolin*

Unirradiated Time (min.)	1	5.5	9	14	29	44	59	74	89	104	Mullite		Final Peak Intensity
											Standard Intensity	Intensity	
It	67		117	130	140	152	152	152	150	150	316		165
Mt	21.2		27.0	41.3	44.3	48.2	48.2	48.2	47.5	47.5			48
Peak Height	2.2		4.3	5.1	5.9	6.4	6.7	6.7	6.8	7.0			7.2
Bo	1.52		1.36	1.26	1.19	1.19	1.13	1.13	1.10	1.07			1.16
<hr/>													
1018ev/gm													
Time (min.)	6	10	13	17	32	47	62	77					
It	110	123	135	145	150	150	148	150			324		155
Mt	34.1	38.0	41.7	44.8	46.5	46.5	45.7	46.5					46.5
Peak Height	4.4	5.3	5.6	6.4	6.4	6.5	6.2	6.2					8.0
Bo	1.25	1.16	1.20	1.13	1.16	1.15	1.16	1.20					0.97
<hr/>													
1019ev/gm													
Time (min.)	2	4.5	9	13	16	31	46	61					
It	117	126	132	133	132	132	134	134			266		140
Mt	44.0	47.5	49.7	50.1	49.7	49.7	50.5	50.5					50.5
Peak Height	5.1	5.7	5.9	6.5	5.6	5.7	6.1	5.9					7.0
Bo	1.14	1.11	1.13	1.03	1.18	1.15	1.10	1.15					1.00
<hr/>													
1020ev/gm													
Time (min.)	2	6.5	9.0	14	29	44	59						
It	100	148	163	181	184	182	186				362		190
Mt	27.6	40.6	45.0	50.0	51.0	50.4	51.3						51.0
Peak Height	3.7	5.9	6.8	7.0	8.3	8.3	8.5						10.0
Bo	1.35	1.25	1.19	1.28	1.11	1.09	1.08						0.95
<hr/>													
1021ev/gm													
Time (min.)	0.5	3	7.5	10.5	15	30	45	60	75				
It	30	47	53	62.5	72	72.5	70	71.5	72		149		72
Mt	20.1	32.5	35.6	42.0	48.3	48.6	47.0	47.8	48.3				48.3
Peak Height	1.4	2.1	2.6	3.0	3.1	3.2	3.3	3.1	3.2				3.7
Bo	1.07	1.14	1.02	1.04	1.16	1.14	1.06	1.14	1.12				0.97
<hr/>													
1022ev/gm													
Time (min.)	2	4.5	9	11	16	31	46	61	76				
It	24.5	27	28.5	32	32	37	35	34.5	35		149		51.5
Mt	24.1	26.6	28.1	31.6	31.6	36.6	34.6	34.1	34.6				34.6
Peak Height	1.0	1.1	1.2	1.4	1.4	1.6	1.6	1.6	1.6				3.0
Bo	1.22	1.22	1.17	1.16	1.16	1.16	1.11	1.11	1.11				0.86

* Explanation of table captions appears on page 47.

Table 4. Mullite Growth--1200°C (Continued)

D. Reproducibility of Medium nb/3-Crystallized Kaolin-- 10^{21} ev/gm^a

No. 1R	Time (min.)	2	4.5	9	11	16	31	46	61	76	Mullite Standard Intensity	Final Peak Intensity
It	43	70	92	120	123	127	130	130	273	130		
Mt	16	26.0	34.2	44.4	45.6	46.8	48.0	47.4				47.6
Peak Height	1.4	2.4	4.0	4.6	4.9	5.8	5.7	6.8				6.8
Bo	1.52	1.44	1.15	1.31	1.23	1.28	1.09	1.10	1.13			0.96
No. 2R	Time (min.)	2	4.5	9	11	16	31	46	61	76		
It	56	71	90	100	110	120	133	133	333	150		
Mt	18.6	23.3	30	33.3	40	43.3	45.0	45.0				45.0
Peak Height	1.16	2.4	3.4	3.6	4.0	5.0	5.4	6.0				6.2
Bo	1.75	1.48	1.32	1.38	1.38	1.20	1.23	1.19	1.10			1.21
No. 3R	Time (min.)	2	4.5	9	11	16	31	46	61	76		
It	72	103	113	126	126	158	165	165	372	180		
Mt	27.2	39.4	45.3	47.4	47.4	48.3	48.9	48.9				48.5
Peak Height	2.9	4.2	5.3	5.8	6.0	6.5	6.7	6.8				7.8
Bo	1.22	1.23	1.06	1.08	1.06	1.21	1.21	1.20	1.20			2.56
No. 4R	Time (min.)	1	3	8	10	15	30	45	60	75		
It	53	72	107	108	118	127	131	126	277	131		
Mt	19.5	30.2	43.3	43.5	46.0	47.8	48.4	46.5				47.3
Peak Height	2.0	3.4	4.3	4.7	5.0	5.1	5.4	5.6				6.1
Bo	1.22	1.06	1.26	1.14	1.18	1.25	1.21	1.18	1.17			1.16
No. 5R	Time (min.)	1	3	8	10	15	30	45	60	75		
It	113	133	135	137	135	135	137	137	304	148		
Mt	40.1	47.3	48.0	48.5	48.0	48.0	48.5	48.5				48.7
Peak Height	4.6	5.7	4.9	4.9	5.0	6.9	6.9	6.8				7.3
Bo	1.23	1.18	1.36	1.35	1.35	0.97	0.98	0.99	1.00			1.00
Standard deviation of Mt (%)	13.0	9.6	7.1	5.0	3.6	2.9	3.1	2.6	2.4			

^a Explanation of table captions appears on page 47.

Table 5. Mollite Growth-1150P

A. Well nb/3-Crystallized Kaoline*

Unirradiated		Mollite Standard Intensity														Final Peak Intensity	
Time (min.)		2	4.5	9	10	16	31	46	61	76	91	106	121	136	151	166	181
10 ¹⁸ ev/gm	It	65	97	92	97	105	118	127	134	141	144	154	166	170	176	174	180
	Mt	17.3	25.8	24.5	25.8	27.9	31.1	33.8	35.6	37.5	38.3	41.0	44.0	45.3	46.7	46.3	47.7
	Peak Height	2.4	2.6	2.8	3.0	3.3	3.6	4.2	4.4	5.0	5.2	5.6	6.0	6.9	6.8	7.5	7.6
	Bo	1.36	1.87	1.54	1.62	1.59	1.85	1.52	1.52	1.41	1.38	1.37	1.38	1.23	1.29	1.18	1.19
10 ¹⁸ ev/gm		2	4.5	9	10	16	31	46	61	76	91	106	121	136	151	166	181
10 ¹⁹ ev/gm	It	80	75	85	85	90	90	95	95	100	100	100	110	110	113	113	115
	Mt	34.5	27.8	36.6	36.6	38.8	38.8	41.0	41.0	43.1	43.1	45.1	47.3	47.3	48.7	48.7	49.5
	Peak Height	2.2	2.3	2.6	2.6	2.8	3.1	2.9	3.3	3.5	3.6	3.6	3.8	4.0	4.0	4.1	4.3
	Bo	1.80	1.63	1.64	1.64	1.60	1.45	1.45	1.44	1.43	1.39	1.39	1.45	1.37	1.38	1.36	1.34
10 ¹⁹ ev/gm		2	4	6	8	10	12	14	16	18	20	22	24	26	30	46	60
10 ²⁰ ev/gm	It	92	100	106	105	107	110	122	125	126	128	132	142	145	138	152	166
	Mt	25.6	27.8	29.5	29.2	29.8	30.6	34.0	34.8	35.1	35.6	36.8	39.5	40.4	38.4	42.3	45.3
	Peak Height	3.6	3.2	3.3	3.6	3.9	3.8	4.1	4.5	4.6	4.9	5.1	5.3	5.7	6.4	6.5	6.5
	Bo	1.28	1.56	1.61	1.47	1.37	1.45	1.50	1.39	1.32	1.31	1.29	1.34	1.27	1.08	1.17	1.28
10 ²⁰ ev/gm		2	4	6	8	10	12	14	16	18	20	22	24	26	30	46	60
10 ²¹ ev/gm	It	72	66	70	73	75	73	72	77	75	74	79	87	88	80	85	85
	Mt	24.8	22.9	24.2	25.2	25.9	25.2	24.8	26.7	25.9	25.5	27.2	30.0	30.3	27.6	29.4	29.4
	Peak Height	1.6	2.0	2.3	2.2	2.2	2.4	2.4	2.5	2.4	2.6	2.6	2.5	2.6	2.6	2.8	2.8
	Bo	2.25	1.65	1.52	1.66	1.70	1.52	1.50	1.54	1.57	1.52	1.52	1.71	1.70	1.54	1.51	1.51
10 ²¹ ev/gm		2	4	6	8	10	12	14	16	18	20	22	24	26	30	46	60
10 ²² ev/gm	It	42	46	47	51	54	56	56	58	58	50	47	47	47	50	53	53
	Mt	27.1	28.4	30.4	26.5	27.8	29.6	29.6	32.0	29.6	32.2	30.4	32.4	32.2	32.2	34.2	34.2
	Peak Height	2.0	2.1	2.4	2.1	2.4	2.4	2.4	2.5	2.5	2.7	2.6	2.8	2.8	2.8	3.2	3.2
	Bo	1.06	1.04	1.01	.99	.90	.96	1.00	.92	1.00	1.00	0.91	0.84	0.89	0.89	0.89	0.88
10 ²² ev/gm		2	4	6	8	10	12	14	16	18	20	22	24	26	30	46	60
10 ²³ ev/gm	It	80	75	88	88	105	100	98	100	100	110	105	107	110	110	114	120
	Mt	22.6	20.6	24.8	24.8	29.6	28.3	27.7	28.3	28.3	31.1	29.6	30.2	31.1	31.1	32.2	33.9
	Peak Height	2.0	2.0	2.7	2.7	3.0	3.1	2.7	3.1	3.1	3.2	3.5	3.2	3.5	3.6	3.7	4.0
	Bo	1.96	1.83	1.63	1.64	1.74	1.62	1.80	1.62	1.62	1.56	1.50	1.67	1.57	1.53	1.54	1.50

* Explanation of table captions appears on page 47.

Table 5. Mullite Growth--1150° (Continued)
B. Medium nb/3-Crystallized Kaolin^a

Unirradiated		Mullite Standard Intensity																Final Peak Intensity											
Time (min.)		1	3	8	10	15	30	45	60	75	90	105	120																
28	It	8.81	10.4	13.5	15.7	17.3	30.5	35.8	36.5	36.2	35.8	36.5	36.2																
0.8	Mt	0.9	1.0	1.2	1.3	1.4	3.6	4.8	5.0	5.2	5.5	5.4	5.4																
0.8	Bo	1.75	1.83	2.15	2.08	1.53	1.34	1.19	1.16	1.13	1.04	1.08	1.08																
<hr/>																													
10 ¹⁸ ev/gm		2	4	6	8	10	12	14	16	18	20	22	24	26	28	30	44	60	74	90	104	120	134	150	164				
63	It	23.6	23.6	22.5	22.5	24.7	24.4	28.1	28.1	28.1	27.4	24.4	28.1	29.2	29.2	32.2	35.6	34.8	35.6	37.4	37.4	38.2	37.4	37.4	100	100	103	-	
0.8	Mt	1.6	1.5	1.4	2.0	1.8	2.2	2.2	2.2	2.1	2.0	1.8	2.0	2.1	2.2	2.5	2.6	2.6	2.9	3.1	3.1	3.4	3.5	3.6	37.4	37.4	37.8	275	
0.8	Bo	1.97	2.10	2.14	1.50	1.63	1.82	1.70	1.70	1.78	1.81	1.80	1.83	1.85	1.80	1.71	1.82	1.79	1.82	1.71	1.51	1.53	1.51	1.42	1.39	1.47	1.47	-	
<hr/>																													
10 ¹⁹ ev/gm		2	4	5	5	8	10	12	14	16	18	20	22	24	26	28	30	44	60	74	90	104	120	134	150	164	184	194	
47	It	16.6	16.0	19.5	21.0	21.0	21.2	21.0	28.4	23.6	21.3	23.1	23.4	23.1	24.8	24.8	27.5	30.1	31.9	32.5	36.7	36.7	38.2	37.8	36.5	37.3	37.8	286	
0.8	Mt	1.4	1.5	1.8	1.9	1.8	1.9	2.1	2.0	1.8	1.8	2.2	2.1	2.1	2.0	2.0	2.0	2.7	2.6	2.7	2.9	2.8	3.2	3.4	3.7	3.7	3.6	3.9	
0.8	Bo	1.68	1.50	1.52	1.52	1.61	1.55	1.38	2.00	1.78	1.66	1.48	1.65	1.62	1.75	1.75	1.45	1.61	1.66	1.55	1.75	1.60	1.58	1.44	1.39	1.43	1.37	1.49	
<hr/>																													
10 ²⁰ ev/gm		2	4	6	8	10	12	14	16	18	20	22	24	26	28	30	44	60	74	90	104	120	134	150	164	180	194	-	
65	It	17.3	15.9	17.0	16.5	19.1	18.1	17.6	17.3	19.1	22.4	21.3	19.7	20.5	20.0	20.2	23.6	22.6	23.9	23.4	27.4	26.6	26.6	26.9	26.9	27.4	120	120	
0.8	Mt	1.9	1.6	1.7	1.8	1.9	2.0	2.2	2.1	2.0	2.4	2.1	2.6	2.7	2.6	2.4	2.8	2.8	3.2	3.3	3.6	3.8	3.8	3.9	4.0	4.0	4.4	4.4	
0.8	Bo	1.71	1.87	1.87	1.72	1.89	1.70	1.59	1.54	1.80	1.73	1.81	1.56	1.41	1.41	1.58	1.87	1.84	1.80	1.38	1.57	1.39	1.32	1.27	1.49	1.28	1.36	1.36	
<hr/>																													
10 ²¹ ev/gm		2	4	6	8	10	12	14	16	18	20	22	24	26	28	30	44	60	74	90	104	120	134	150	164	180	194	-	
52	It	15.3	15.6	17.6	19.1	18.2	19.7	19.4	18.2	18.5	17.6	18.2	19.4	19.1	20.0	20.0	22.5	24.0	25.0	25.6	28.5	28.5	29.4	29.4	30.0	29.4	100	100	
0.8	Mt	1.4	1.2	1.2	1.2	1.3	1.7	1.8	1.7	1.7	1.8	1.8	1.8	1.8	1.9	1.9	2.2	2.3	2.7	2.8	2.8	2.8	2.8	2.8	2.8	2.8	29.4	29.4	
0.8	Bo	1.85	2.20	2.50	2.70	2.38	1.97	1.83	1.82	1.84	1.67	1.68	1.71	1.70	1.78	1.78	1.70	1.78	1.74	1.78	1.61	1.63	1.79	1.58	1.50	1.52	1.39	1.39	
<hr/>																													
10 ²² ev/gm		2	4	6	8	10	12	14	16	18	20	22	24	26	28	30	44	60	74	90	104	120	134	150	164	180	194	-	
55	It	11.6	12.6	11.6	13.3	12.4	12.6	13.3	13.1	12.6	12.6	13.1	13.3	13.6	13.3	15.0	15.8	15.8	16.8	15.8	19.2	20.2	21.1	21.1	21.1	100	100	100	
0.8	Mt	1.4	1.6	1.7	1.6	1.6	1.6	1.6	1.6	1.6	1.6	1.6	1.8	1.7	1.7	2.0	2.4	2.5	3.0	3.1	3.4	3.7	3.7	3.7	3.6	3.4	21.1	21.1	
0.8	Bo	1.96	1.87	1.61	1.96	1.84	1.87	1.75	1.94	1.87	1.87	1.88	1.89	1.76	1.88	1.78	1.56	1.53	1.66	1.66	1.86	1.60	1.47	1.35	1.39	1.18	1.22	1.22	
<hr/>																													

Table 5. Mullite Growth--1150°
C. Poorly nb/3-Crystallized Kaolin*

Unirradiated		Time (min.)														Mullite Standard Intensity		Final Peak Intensity
10 ¹⁸ ev/gm		2	4.5	9	11	16	31	46	61	76	91	106	121	136	142	151	-	
I _c	63	70	71	75	85	90	95	97	107	115	118	115	119	120		407	125	
M _c	15.5	16.3	18.2	18.4	19.4	22.0	23.3	24.6	25.1	27.8	29.8	30.4	29.8	30.8	31.1		30.4	
Peak Height	1.5	1.6	2.3	1.9	2.2	2.6	6.6	6.4	6.8	8.0	8.1	8.8	8.8	8.8	8.8		9.6	
Bo	2.00	1.97	1.52	1.86	1.70	1.64	1.60	1.48	1.43	0.79	0.72	0.74	0.65	0.67	0.68		0.65	
10 ¹⁹ ev/gm		2	6.5	9	14	29	44	59	74	89	104	119	134	149	164	174	-	
I _c	48	48	57	57	72	78	75	90	90	94	90	97	94	95	96	95	275	
M _c	17.7	17.7	21.0	21.0	26.6	28.8	27.8	33.3	33.3	33.3	38.9	38.9	38.7	35.3	35.5	35.3	35.3	
Peak Height	1.6	1.6	1.8	2.0	2.2	2.2	2.2	2.5	2.5	2.5	2.9	2.9	3.1	2.9	3.0		3.2	
Bo	1.50	1.50	1.59	1.42	1.63	1.76	1.87	1.80	1.60	1.61	1.67	1.62	1.53	1.63	1.58		1.51	
10 ²⁰ ev/gm		1	3	8	10	15	30	45	60	75	90	105	120	135	150	165	180	
I _c	80	100	100	137	135	162	176	196	216	234	234	244	250	240	244	246	242	
M _c	12.8	15.9	15.9	21.8	21.4	25.9	27.9	31.1	34.3	37.1	37.1	38.8	39.7	38.2	38.8	39.0	34.8	
Peak Height	2.2	4.8	4.3	4.3	4.9	5.9	6.5	8.0	9.2	9.3	10.1	10.0	10.5	10.4	10.8	11.00	10.4	
Bo	1.82	1.78	1.35	1.59	1.40	1.37	1.35	1.23	1.17	1.26	1.15	1.22	1.19	1.14	1.11	1.11	1.11	
10 ²¹ ev/gm		1	3	8	10	15	30	45	60	75	90	105	120	135	150	165	180	
I _c	72	80	87	95	100	112	118	128	139	137	143	150	160	160	164	170	160	
M _c	18.1	20.1	21.8	23.8	25.1	28.1	29.6	32.1	35.0	34.5	35.8	37.7	40.3	40.3	41.2	42.7	40.3	
Peak Height	2.4	2.6	3.0	3.3	3.6	4.0	4.4	4.9	4.8	4.8	5.6	6.0	5.6	5.6	6.8	7.2	7.4	
Bo	1.50	1.54	1.68	1.58	1.51	1.55	1.47	1.43	1.41	1.42	1.28	1.20	1.47	1.21	1.23	1.09	1.06	
10 ²² ev/gm		1	3	8	10	15	30	45	60	75	90	105	120	135	150	165	180	
I _c	63	79	96	99	100	111	115	125	132	130	140	150	158	170	170	174	180	
M _c	17.1	16.3	19.8	20.4	20.6	22.9	23.7	25.8	27.2	26.8	28.9	30.9	32.6	35.0	35.0	35.5	36.7	
Peak Height	2.1	2.1	2.7	2.8	2.9	3.5	3.8	4.3	4.6	4.8	5.5	6.0	6.6	6.6	6.8	7.4	7.4	
Bo	1.80	1.88	1.81	1.77	1.73	1.58	1.51	1.45	1.41	1.12	1.06	1.03	1.02	1.36	1.24	1.15	1.28	
10 ²³ ev/gm		2	4.5	9	11	16	31	46	61	76	91	106	121	136	151	166	181	
I _c	77	87	91	93	98	100	103	108	115	125	125	132	140	148	150	164	164	
M _c	16.9	19.1	20.0	20.4	21.5	22.0	22.6	23.8	25.3	27.5	28.8	30.1	32.3	33.0	36.0	36.0	36.0	
Peak Height	2.4	2.6	2.9	2.9	3.2	3.6	3.6	4.5	4.4	4.6	5.0	4.9	5.7	6.0	6.8	6.6	6.6	
Bo	1.60	1.67	1.56	1.66	1.68	1.72	1.42	1.50	1.28	1.42	1.43	1.40	1.50	1.32	1.37	1.37	1.25	

Table 6. Mullite Growth--1100°C
A. Well nb/3-crystallized Kaelin^a

Unirradiated		Mullite Standard		Peak Intensity	
Time (min.)	2	4	6	8	10
Time (min.)	2	4	6	8	10
Peak Height	1.57	1.65	1.63	1.65	1.54
Bo	1.57	1.65	1.63	1.65	1.54
10 ¹⁸ ev/gm					
Time (min.)	2	4	6	8	10
Time (min.)	2	4	6	8	10
Peak Height	1.82	2.00	1.80	1.84	2.00
Bo	1.82	2.00	1.80	1.84	2.00
10 ¹⁹ ev/gm					
Time (min.)	2	4	6	8	10
Time (min.)	2	4	6	8	10
Peak Height	1.68	2.00	1.71	1.59	1.75
Bo	1.68	2.00	1.71	1.59	1.75
10 ²⁰ ev/gm					
Time (min.)	2	4	6	8	10
Time (min.)	2	4	6	8	10
Peak Height	1.61	1.80	1.51	1.71	1.87
Bo	1.61	1.80	1.51	1.71	1.87
10 ²¹ ev/gm					
Time (min.)	2	4	6	8	10
Time (min.)	2	4	6	8	10
Peak Height	1.78	2.14	1.97	1.92	1.78
Bo	1.78	2.14	1.97	1.92	1.78
10 ²² ev/gm					
Time (min.)	2	4	6	8	10
Time (min.)	2	4	6	8	10
Peak Height	1.78	2.14	1.97	1.92	1.78
Bo	1.78	2.14	1.97	1.92	1.78

^a Explanation of table captions appears on page 47.

Table 6. Mullite Growth--100° C (Continued)

B. Medium nb/s-Crystallized Koolin*

Unirradiated Time (min.)	2	4	6	8	10	12	14	16	18	20	22	24	26	28	30	32	34	36	38	40	42	44	46	48	50	52	54	56	58	60	62	64	66	68	70	72	74	76	78	80	82	84	86	88	90	92	94	96	98	100	102	104	106	108	110	112	114	116	118	120	122	124	126	128	130	132	134	136	138	140	142	144	146	148	150	152	154	156	158	160	162	164	166	168	170	172	174	176	178	180	182	184	186	188	190	192	194	196	198	200	202	204	206	208	210	212	214	216	218	220	222	224	226	228	230	232	234	236	238	240	242	244	246	248	250	252	254	256	258	260	262	264	266	268	270	272	274	276	278	280	282	284	286	288	290	292	294	296	298	300	302	304	306	308	310	312	314	316	318	320	322	324	326	328	330	332	334	336	338	340	342	344	346	348	350	352	354	356	358	360	362	364	366	368	370	372	374	376	378	380	382	384	386	388	390	392	394	396	398	400	402	404	406	408	410	412	414	416	418	420	422	424	426	428	430	432	434	436	438	440	442	444	446	448	450	452	454	456	458	460	462	464	466	468	470	472	474	476	478	480	482	484	486	488	490	492	494	496	498	500	502	504	506	508	510	512	514	516	518	520	522	524	526	528	530	532	534	536	538	540	542	544	546	548	550	552	554	556	558	560	562	564	566	568	570	572	574	576	578	580	582	584	586	588	590	592	594	596	598	600	602	604	606	608	610	612	614	616	618	620	622	624	626	628	630	632	634	636	638	640	642	644	646	648	650	652	654	656	658	660	662	664	666	668	670	672	674	676	678	680	682	684	686	688	690	692	694	696	698	700	702	704	706	708	710	712	714	716	718	720	722	724	726	728	730	732	734	736	738	740	742	744	746	748	750	752	754	756	758	760	762	764	766	768	770	772	774	776	778	780	782	784	786	788	790	792	794	796	798	800	802	804	806	808	810	812	814	816	818	820	822	824	826	828	830	832	834	836	838	840	842	844	846	848	850	852	854	856	858	860	862	864	866	868	870	872	874	876	878	880	882	884	886	888	890	892	894	896	898	900	902	904	906	908	910	912	914	916	918	920	922	924	926	928	930	932	934	936	938	940	942	944	946	948	950	952	954	956	958	960	962	964	966	968	970	972	974	976	978	980	982	984	986	988	990	992	994	996	998	1000																																																																																																																																																																																																																																																																																																																																																																																																																																										
Peak Height	1.8	2.0	2.1	2.2	2.3	2.4	2.5	2.6	2.7	2.8	2.9	3.0	3.1	3.2	3.3	3.4	3.5	3.6	3.7	3.8	3.9	4.0	4.1	4.2	4.3	4.4	4.5	4.6	4.7	4.8	4.9	5.0	5.1	5.2	5.3	5.4	5.5	5.6	5.7	5.8	5.9	6.0	6.1	6.2	6.3	6.4	6.5	6.6	6.7	6.8	6.9	7.0	7.1	7.2	7.3	7.4	7.5	7.6	7.7	7.8	7.9	8.0	8.1	8.2	8.3	8.4	8.5	8.6	8.7	8.8	8.9	9.0	9.1	9.2	9.3	9.4	9.5	9.6	9.7	9.8	9.9	10.0	10.1	10.2	10.3	10.4	10.5	10.6	10.7	10.8	10.9	11.0	11.1	11.2	11.3	11.4	11.5	11.6	11.7	11.8	11.9	12.0	12.1	12.2	12.3	12.4	12.5	12.6	12.7	12.8	12.9	13.0	13.1	13.2	13.3	13.4	13.5	13.6	13.7	13.8	13.9	14.0	14.1	14.2	14.3	14.4	14.5	14.6	14.7	14.8	14.9	15.0	15.1	15.2	15.3	15.4	15.5	15.6	15.7	15.8	15.9	16.0	16.1	16.2	16.3	16.4	16.5	16.6	16.7	16.8	16.9	17.0	17.1	17.2	17.3	17.4	17.5	17.6	17.7	17.8	17.9	18.0	18.1	18.2	18.3	18.4	18.5	18.6	18.7	18.8	18.9	19.0	19.1	19.2	19.3	19.4	19.5	19.6	19.7	19.8	19.9	20.0	20.1	20.2	20.3	20.4	20.5	20.6	20.7	20.8	20.9	21.0	21.1	21.2	21.3	21.4	21.5	21.6	21.7	21.8	21.9	22.0	22.1	22.2	22.3	22.4	22.5	22.6	22.7	22.8	22.9	23.0	23.1	23.2	23.3	23.4	23.5	23.6	23.7	23.8	23.9	24.0	24.1	24.2	24.3	24.4	24.5	24.6	24.7	24.8	24.9	25.0	25.1	25.2	25.3	25.4	25.5	25.6	25.7	25.8	25.9	26.0	26.1	26.2	26.3	26.4	26.5	26.6	26.7	26.8	26.9	27.0	27.1	27.2	27.3	27.4	27.5	27.6	27.7	27.8	27.9	28.0	28.1	28.2	28.3	28.4	28.5	28.6	28.7	28.8	28.9	29.0	29.1	29.2	29.3	29.4	29.5	29.6	29.7	29.8	29.9	30.0	30.1	30.2	30.3	30.4	30.5	30.6	30.7	30.8	30.9	31.0	31.1	31.2	31.3	31.4	31.5	31.6	31.7	31.8	31.9	32.0	32.1	32.2	32.3	32.4	32.5	32.6	32.7	32.8	32.9	33.0	33.1	33.2	33.3	33.4	33.5	33.6	33.7	33.8	33.9	34.0	34.1	34.2	34.3	34.4	34.5	34.6	34.7	34.8	34.9	35.0	35.1	35.2	35.3	35.4	35.5	35.6	35.7	35.8	35.9	36.0	36.1	36.2	36.3	36.4	36.5	36.6	36.7	36.8	36.9	37.0	37.1	37.2	37.3	37.4	37.5	37.6	37.7	37.8	37.9	38.0	38.1	38.2	38.3	38.4	38.5	38.6	38.7	38.8	38.9	39.0	39.1	39.2	39.3	39.4	39.5	39.6	39.7	39.8	39.9	40.0	40.1	40.2	40.3	40.4	40.5	40.6	40.7	40.8	40.9	41.0	41.1	41.2	41.3	41.4	41.5	41.6	41.7	41.8	41.9	42.0	42.1	42.2	42.3	42.4	42.5	42.6	42.7	42.8	42.9	43.0	43.1	43.2	43.3	43.4	43.5	43.6	43.7	43.8	43.9	44.0	44.1	44.2	44.3	44.4	44.5	44.6	44.7	44.8	44.9	45.0	45.1	45.2	45.3	45.4	45.5	45.6	45.7	45.8	45.9	46.0	46.1	46.2	46.3	46.4	46.5	46.6	46.7	46.8	46.9	47.0	47.1	47.2	47.3	47.4	47.5	47.6	47.7	47.8	47.9	48.0	48.1	48.2	48.3	48.4	48.5	48.6	48.7	48.8	48.9	49.0	49.1	49.2	49.3	49.4	49.5	49.6	49.7	49.8	49.9	50.0	50.1	50.2	50.3	50.4	50.5	50.6	50.7	50.8	50.9	51.0	51.1	51.2	51.3	51.4	51.5	51.6	51.7	51.8	51.9	52.0	52.1	52.2	52.3	52.4	52.5	52.6	52.7	52.8	52.9	53.0	53.1	53.2	53.3	53.4	53.5	53.6	53.7	53.8	53.9	54.0	54.1	54.2	54.3	54.4	54.5	54.6	54.7	54.8	54.9	55.0	55.1	55.2	55.3	55.4	55.5	55.6	55.7	55.8	55.9	56.0	56.1	56.2	56.3	56.4	56.5	56.6	56.7	56.8	56.9	57.0	57.1	57.2	57.3	57.4	57.5	57.6	57.7	57.8	57.9	58.0	58.1	58.2	58.3	58.4	58.5	58.6	58.7	58.8	58.9	59.0	59.1	59.2	59.3	59.4	59.5	59.6	59.7	59.8	59.9	60.0	60.1	60.2	60.3	60.4	60.5	60.6	60.7	60.8	60.9	61.0	61.1	61.2	61.3	61.4	61.5	61.6	61.7	61.8	61.9	62.0	62.1	62.2	62.3	62.4	62.5	62.6	62.7	62.8	62.9	63.0	63.1	63.2	63.3	63.4	63.5	63.6	63.7	63.8	63.9	64.0	64.1	64.2	64.3	64.4	64.5	64.6	64.7	64.8	64.9	65.0	65.1	65.2	65.3	65.4	65.5	65.6	65.7	65.8	65.9	66.0	66.1	66.2	66.3	66.4	66.5	66.6	66.7	66.8	66.9	67.0	67.1	67.2	67.3	67.4	67.5	67.6	67.7	67.8	67.9	68.0	68.1	68.2	68.3	68.4	68.5	68.6	68.7	68.8	68.9	69.0	69.1	69.2	69.3	69.4	69.5	69.6	69.7	69.8	69.9	70.0	70.1	70.2	70.3	70.4	70.5	70.6	70.7	70.8	70.9	71.0	71.1	71.2	71.3	71.4	71.5	71.6	71.7	71.8	71.9	72.0	72.1	72.2	72.3	72.4	72.5	72.6	72.7	72.8	72.9	73.0	73.1	73.2	73.3	73.4	73.5	73.6	73.7	73.8	73.9	74.0	74.1	74.2	74.3	74.4	74.5	74.6	74.7	74.8	74.9	75.0	75.1	75.2	75.3	75.4	75.5	75.6	75.7	75.8	75.9	76.0	76.1	76.2	76.3	76.4	76.5	76.6	76.7	76.8	76.9	77.0	77.1	77.2	77.3	77.4	77.5	77.6	77.7	77.8	77.9	78.0	78.1	78.2	78.3	78.4	78.5	78.6	78.7	78.8	78.9	79.0	79.1	79.2	79.3	79.4	79.5	79.6	79.7	79.8	79.9	80.0	80.1	80.2	80.3	80.4	80.5	80.6	80.7	80.8	80.9	81.0	81.1	81.2	81.3	81.4	81.5	81.6	81.7	81.8	81.9	82.0	82.1	82.2	82.3	82.4	82.5	82.6	82.7	82.8	82.9	83.0	83.1	83.2	83.3	83.4	83.5	83.6	83.7	83.8	83.9	84.0	84.1	84.2	84.3	84.4	84.5	84.6	84.7	84.8	84.9	85.0	85.1	85.2	85.3	85.4	85.5	85.6	85.7	85.8	85.9	86.0	86.1	86.2	86.3	86.4	86.5	86.6	86.7	86.8	86.9	87.0	87.1	87.2	87.3	87.4	87.5	87.6	87.7	87.8	87.9	88.0	88.1	88.2	88.3	88.4	88.5	88.6	88.7	88.8	88.9	89.0	89.1	89.2	89.3	89.4	89.5	89.6	89.7	89.8	89.9	90.0	90.1	90.2	90.3	90.4	90.5	90.6	90.7	90.8	90.9	91.0	91.1	91.2	91.3	91.4	91.5	91.6	91.7	91.8	91.9	92.0	92.1	92.2	92.3	92.4	92.5	92.6	92.7	92.8	92.9	93.0	93.1	93.2	93.3	93.4	93.5	93.6	93.7	93.8	93.9	94.0	94.1	94.2	94.3	94.4

APPENDIX D

ATTEMPTS TO DETERMINE THE MULLITE ACTIVATION ENERGY

Attempts were made to determine the mullite activation energy by both the graphical method and computer programming of the decay product equation (third order). Both attempts were unsuccessful.

In the graphical method the specific rate constant " k_c " of mullite formation was determined by

$$k_c = (1/M)(dM/dt) \quad (7)$$

where $M = M_f = M_t$ (remaining amount of mullite to be formed).

M_f = Final amount of mullite.

M_t = Amount of mullite at time t .

The mullite activation energy may be found by the Arrhenius equation.

$$k_c = R e^{-E/RT} \quad (8)$$

where k_c = Specific rate constant.

R = Constant for particular process.

E = Activation energy.

B = Boltzman's constant (1.38×10^{-16} ergs/ $^{\circ}$ K/molecule).

T = Absolute temperature ($^{\circ}$ K).

Ordinarily the values of " k_c " would be determined from the slope of

semilog plots of (M) versus time. In this case the values of (M) obtained from the diffraction pattern included varying quantities of both mullite and sillimanite. The amount of each phase present could not be resolved for plotting.

Computer programming of the third order Bateman equation (28) was considered as a possible method of determining the sillimanite and mullite growth rate constants and activation energies. The general Bateman equation applies to phase changes of the type Phase A \rightarrow Phase B \rightarrow . . . Phase N, and is as follows:

$$I_N = A_O(h_A e^{-k_A t} + h_B e^{-k_B t} + \dots h_M e^{-k_M t} + h_N e^{-k_N t}) \quad (9)$$

Where I_N = Amount of phase N accumulated (as observed from the diffractometer pattern in this case).

A_O = Amount of phase A (original phase) present at time $t = 0$.

k_A = Growth rate constant of phase B. Phase B may be classed as a first order or daughter product.

k_B = Growth rate constant of phase C. Phase C may be classed as a second order or granddaughter product.

k_M = Growth rate constant of phase N.

k_N = Decay rate constant of phase N. If phase N is stable,

$$k_N = 0.$$

$$h_A = \left(\frac{k_A}{k_C - k_A} \right) \left(\frac{k_B}{k_B - k_A} \right)$$

$$h_B = \left(\frac{k_A}{k_A - k_B} \right) \left(\frac{k_B}{k_C - k_B} \right)$$

$$h_N = \left(\frac{k_A}{k_A - k_N}\right) \left(\frac{k_B}{k_B - k_N}\right) \left(\frac{k_C}{k_C - k_N}\right) \cdot \cdot \cdot \left(\frac{k_M}{k_M - k_N}\right)$$

In the kaolinite-mullite transformation series the formation of the spinel phase is analogous to the formation of Phase B, sillimanite to the formation of Phase C, and mullite to Phase D. Since the sillimanite and mullite reflections could not be resolved, the third order (great granddaughter) product equation was modified to reflect the quantities of both phases present.

$$I_{(C+D)} = K \left[\left(\frac{k_B}{k_A - k_B}\right) \left(\frac{k_C - Wk_A}{k_C - k_A}\right) e^{-k_A t} + \left(\frac{k_A}{k_B - k_A}\right) \left(\frac{k_C - Wk_B}{k_C - k_B}\right) e^{-k_B t} \right. \\ \left. + \frac{k_A k_B (1 - W)}{(k_A - k_C)(k_C - k_B)} e^{-k_C t} + 1 \right] \quad (10)$$

where $I_{(C+D)}$ = Intensity of unresolved sillimanite plus mullite peak at time "t", as observed from a diffractometer pattern.

K = Overall scaling constant.

$W = I_C/I_D$, where I_C is the integrated intensity of the main sillimanite reflection; I_D is the integrated intensity of the main mullite reflection; these intensity values are those obtained from "pure" samples of each.

This equation was coupled with equation 8 for programming purposes. Two separate computer programs were used in an attempt to adjust the parameters of equation 10 to obtain a fit to observed data.

In the first program a least squares fit of equation (10) to the observations (including standard deviation of the fit) was attempted. The General Least Squares program of Busing and Levy (29) was utilized

for this purpose; adaptations for use with the experimental data were proposed by Dr. M. Kay, of the Georgia Institute of Technology Experiment Station. Initially the derivatives needed for the program were determined manually by Dr. Kay. After nonsensical computer solutions were obtained with this approach, the derivatives were calculated analytically by the program subroutine. The program was evaluated both with and without an observation weighting factor. Seven cycles of refinement were intended for convergence to a final solution. Results usually became nonsensical on the second or third cycle. This failure was probably due to inadequate experimental precision.

For use in the second program, specially written by D. J. Parrish of the Lockheed-Georgia Company, equation (10) was simplified to the following form:

$$I_{(C+D)} = K (L_A e^{-k_A t} + L_B e^{-k_B t} + L_C e^{-k_C t} + 1). \quad (11)$$

Evaluating this equation at $t = 0$ we find $K = -(L_A + L_B + L_C)$.

Therefore equation 11 can be simplified:

$$I_{(C+D)} = F e^{-k_A t} + G e^{-k_B t} + H e^{-k_C t} \quad (12)$$

Four values within a wide arbitrary range were then selected for each variable. By testing all, the program selected that combination of values which minimized the function

$$\sum |f(t) - I_{(C+D)}(t)| \quad (13)$$

where $f(t)$ was the fitted value, $I_{(C+D)}(t)$ was the observed value (data) within the range specified. With each cycle the program proposed a new selection of values in a smaller range for each variable and again minimized the function within the choices available. In general the activation energies obtained were not realistic and many were nonsensical (e. g., negative). The poor results were probably due to inadequately broad initial ranges and unresolved program errors.

All program computations were made on the Lockheed-Georgia Company's IBM 7094 computer.

BIBLIOGRAPHY

LITERATURE CITED

1. Brindley, G. W., X-Ray Identification and Structure of the Clay Minerals, Mineralogical Society of Great Britain Monograph, 1951, pp. 32-75.
2. Grim, R. E., Clay Mineralogy, McGraw-Hill Book Co., Inc., 1953, p. 46.
3. Brindley, G. W. and K. Robinson, "Randomness in the Structures of Kaolinite Clay Minerals," Transactions of the Faraday Society, 42B, pp. 198-205.
4. Seitz, F., "Color Centers in Alkali Halide Crystals II," Review of Modern Physics, 26, 1954, p. 1.
5. Murray, H. H., "Structure Variations of Some Kaolinites in Relation to Dehydrated Halloysite," American Mineralogist, 39, 1954, p. 108.
6. Brindley, "Identification by X-ray Analysis," p. 45.
7. Johns, W. D. and H. H. Murray, "An Empirical Index for Kaolinite Crystallinity," paper presented at meeting of Mineralogical Society of America, 1959.
8. Brindley, G. W. M. Nakahira, "The Kaolinite-Mullite Reaction Series," Journal of the American Ceramic Society, 42, 1959, pp. 314-24.
9. Ibid., p. 320.
10. Ibid., p. 322.
11. Ibid., p. 323.
12. Durovic, S., "A Statistical Model for the Crystal Structure of Mullite," Soviet Physics-Crystallography, 7, 1962, pp. 271-78.
13. Parmalee, C. W. and A. R. Podriquer, "Catalytic Mullitization of Kaolinite by Metallic Oxides," Journal of the American Ceramic Society, 25, 1942, pp. 1-10.

14. Johns, W. D., "High-Temperature Phase Changes in Kaolinite," The Mineralogical Magazine and the Journal of the Mineralogical Society, 30, 1955, pp. 186-98.
15. Stourdzé, V. Y., and B. N. F. Nicot, "Mullitization of Tubular Kaolin," Ceramica, (San Paula), 3, 1957, pp. 73-96.
16. Comefero, J. E., R. B. Fischer, and W. F. Bradley, "Mullitization of Kaolinite," Journal of the American Ceramic Society, 31, 1948, pp. 254-59.
17. Comer, J. J., "Electron Microscope Studies of Mullite Development in Fired Kaolinite," Journal of the American Ceramic Society, 43, 1960, pp. 378-84.
18. Brindley and Nakahira, "Reaction Series," p. 314.
19. Carter, R. W. and R. C. Palmer, Cesium-137 Research Irradiator, Quarterly Technical Status Report No. 4, Georgia Institute of Technology, 1960, pp. 8-15.
20. Johns and Murray, op. cit.
21. Krueger, H. H. A. and W. R. Cook, "Radiation Damage in the Ferroelectric Effect in Rochelle Salt," Journal of Applied Physics, 34, 1963, pp. 218-24.
22. Brindley and Nakahira, "Reaction Series," p. 314.
23. Comer, J. J., "New Electron-Optical Data on the Kaolinite-Mullite Transformation," Journal of the American Ceramic Society, 44, 1964, pp. 561-563.
24. Brindley and Nakahira, "Reaction Series," p. 314.
25. Comer, op. cit., p. 562.
26. Comer, "Electron Microscope Studies of Mullite Development," p. 379.
27. Parmalee, op. cit., p. 10.
28. Evans, R. D., The Atomic Nucleus, McGraw-Hill Book Co., Inc., 1955, pp. 490-492.
29. Busing, W. R., and Levy, H. A., A General Fortran Least Squares Program, report No. ORNL-TM-271, Oak Ridge National Laboratory, 1962.